5-2016

Impact of Extreme Summer Temperatures on Bridge Structures

Ryan Hagedorn
University of Arkansas, Fayetteville

Impact of Extreme Summer Temperatures on Bridge Structures

A thesis submitted in partial fulfillment
of the requirements for the degree of
Master of Science in Civil Engineering

by

Ryan Hagedorn
University of Arkansas
Bachelor of Science in Civil Engineering, 2014

May 2016
University of Arkansas

This thesis is approved for recommendation to the Graduate Council.

_____
Dr. W. Micah Hale
Thesis Director

_____
Dr. Gary Prinz
Committee Member

_____
Dr. Canh Dang
Committee Member

Abstract

Climate change and its effect on weather in the United States is a well-documented phenomenon. In particular, extreme heat waves have become more intense, more frequent, and longer lasting, especially in the southern United States. As with much of America's transportation infrastructure, prestressed concrete bridge girders experience the effects of these heat waves. Uneven heating of optimized bridge girder sections results in large non-linear temperature gradients. In this study, temperature was monitored in three different AASHTO I-girders to determine the vertical and transverse temperature gradients in a pre-deck placement condition. It was determined that the current design standard, which uses a non-linear vertical thermal gradient, was inaccurate in both shape and magnitude for girders Type IV and smaller in this condition. Transverse gradients were also recommended as none are included in design standards. Using three dimensional modeling, this study also sought to understand the response of the girders to non-linear temperature gradients and if they should be accounted for in girder design.

Table of Contents

List of Figures

List of Tables

1. Introduction

1.1. Research Motivation

Worldwide climate change has been observed and studied extensively, research suggesting that heat waves are becoming more intense, longer lasting, and more frequent (Meehl & Tebaldi, 2004; Schwartz, 2010). The effects of climate change on America's infrastructure and transportation systems are of particular concern for engineers. Heat waves can affect thermal expansion joints, accelerate material degradation, and increase stresses in concrete bridge girders. In particular, optimized bridge girder sections, such as box girders and I-beams, experience the effects of heat waves due to the large temperature variations throughout their section shapes. Numerous investigations, which will be discussed in detail in following sections, indicate an increase in stress in both the tension and compression regions of concrete bridge girders due to temperature gradients. These stresses can reduce the serviceability and durability of bridges by initiating new cracks or widening existing cracks, therefore accelerating steel deterioration through corrosion. In some cases, stresses caused by thermal gradients can decrease the stability of bridge structures (Oesterle, Sheehan, Lotfi, Corley, & Roller, 2007). Recent research has also explored how temperature profiles may affect camber of prestressed concrete girders (Nguyen, Stanton, Eberhard, & Chapman, 2015). For these reasons, it is important to analyze past efforts in this field and examine current design standards and practices.

Because of constant exposure to environmental conditions, bridge girders experience large temperature variations. Temperature gradients can be observed in the longitudinal, transverse, and vertical directions. In most cases, temperature change in the longitudinal direction is considered to be uniform, but variable in the transverse and vertical directions (Ghali, Favre, & Eldbadry, 2006). In simple spans, or statically determinate structures, longitudinal

temperature change is generally accounted for by bearing pads and expansion joints that allow expansion and contraction. In statically indeterminate structures, longitudinal temperature variations produce additional stresses that must be accounted for during design. (Ghali et al., 2006) This study focuses on the response of simple span structures.

This research is concerned with how temperature varies over the depth and width of commonly used bridge sections, requiring the fundamental mechanisms of heat transfer in bridge girders to be understood. The main mechanisms are absorption of solar radiation and convection from ambient air temperature (Ghali et al., 2006). Solar radiation is simply a function of the time of day, time of year, amount of sunlight, and angle and orientation of the surface being observed. Girders can also absorb reflected solar radiation from surrounding surfaces in which case the distance and properties of the reflecting surface would be contributing factors. The convection heat is dependent on factors such as air temperature and wind speed. The changes in ambient air temperature contribute mostly to temperature change in the longitudinal direction of bridges (normally accounted for with expansion joints and bearing pads) only producing stress in statically indeterminate structures. Solar radiation, however, affects cross sections regardless of support conditions. The exposed surfaces are heated, and in the case of cross sections that are optimized for minimal material with maximum moment capacity, non-linear temperature gradients are produced. Non-linear temperature gradients produce the thermal stresses which can affect bridge structures in the previously mentioned manners. Figure 1.1 displays the main mechanisms of heat transfer to concrete bridge structures.

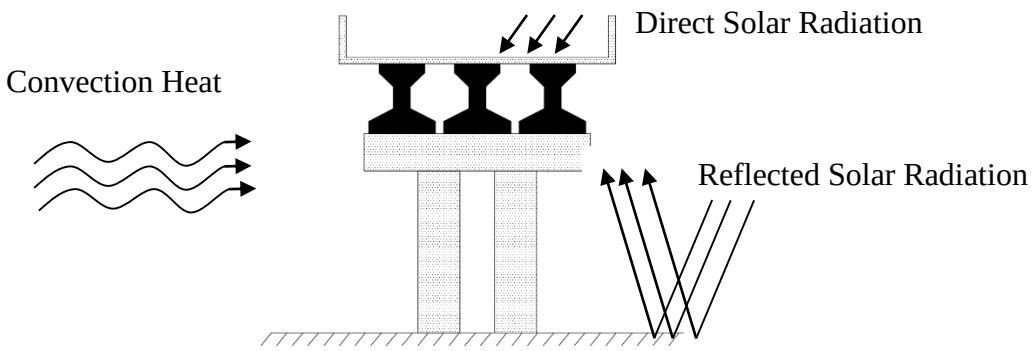

Figure 1.1 - Heat Transfer Mechanisms

Non-linear vertical temperature gradients can lead to durability and serviceability concerns in the form of widening of existing cracks and creation of new cracks. Extensive research, while not all-encompassing, has been done in this area. There is not a comprehensive understanding of what vertical gradients look like in different section shapes, but the basic overall effects of vertical gradients are generally well documented. However, stability concerns arise from transverse gradients, which are mentioned sparingly in previous research. There are two events that demonstrate the need to better understand transverse thermal gradients: a collapse of bridge girders in Pennsylvania in 2004, and a similar collapse of a section of bridge girders in Arizona in 2007. In the fall of 2004, prestressed girders that were 7'6" deep, 2'4" wide, and spanned 150 feet, collapsed during the construction phase, prior to placement of the bridge deck. A possible contributing cause of the collapse was uneven heating of the girders contributing to lateral instability (Hurff, 2010). This failure is depicted Figure 1.2.

Figure 1.2 - Collapse of I-80 girders in Pennsylvania (Hurff, 2010)

In the summer of 2007, there was a similar failure of a section of bridge girders on the Red Mountain Freeway in Mesa, Arizona. This event is pictured in Figure 1.3. The collapse happened during construction, before placement of the bridge deck. The failed section spanned 114 feet with American Association of State Highway and Transportation Officials (AASHTO) Type V prestressed girders, which have a depth of 5'3" and a width of 2'4". Investigators concluded that the collapse was caused by the lateral instability of one member, which triggered a chain reaction in the adjacent girders. Among other factors, such as bearing eccentricity, support slopes, and construction imperfections, thermal sweep was cited as a major contributing factor (Oesterle et al., 2007). Thermal sweep occurs when one side of a girder is heated by solar radiation and causes lateral bowing and instability.

Figure 1.3 - Collapse Red Mountain Freeway girders in Arizona (Oesterle et al., 2007)

Both of the collapses described above occurred on bridges using I-girders and cited temperature gradients are one of the contributing causes of failure. Current AASHTO design standards are based off research completed on box girder sections and neglect to address transverse gradients at all. The most recent data published by the United States Federal Highway Administration states that, in 2014, there were approximately 610,000 highway bridges in the United States. Of those bridges, approximately 405,000 had concrete superstructures, or approximately 66% of all highway bridges were constructed of concrete. Of concrete bridges, non-box girder bridges accounted for approximately 63% of concrete bridges or 42% of all American highway bridges. These events and the wide usage of concrete girders that are not box girders demonstrate the need to better understand the temperature distribution in bridge girder sections being used today such as I-shaped girders.

1.2. Research Goals

The goal of this research is to investigate temperature distributions in concrete AASHTO I-girders. Temperature will be recorded in three different section shapes to determine maximum vertical and transverse thermal gradients. Often temperature gradients are maximized during the bridge construction phase, before the placement of a bridge deck; therefore, the experimental segments in this study will be monitored without a deck. This study will establish the environmental conditions that result in these gradients with particular interest in the impact of extreme heat events. Additionally, the global response of full scale girders to thermal gradients will be investigated using three-dimensional finite element modeling. The measured thermal gradients will be compared against design gradients in this step. Temperature gradients have the ability to increase compressive and tensile stresses in girders as well as affect lateral stability. Ultimately, the goal of this research is to determine if temperature gradients are more extreme due to extreme heat events and if design procedures need to be altered to account for these gradients.

2. Previous Research

2.1. Thermal Properties of Concrete

Different concrete mixtures possess different thermal properties. An important question to ask when studying the temperature gradients in concrete structures then is how these properties affect thermal response. The main contributing thermal factor that could affect temperature gradients is the thermal conductivity of concrete. Thermal conductivity is the rate that heat flows by conduction through a material. Specific heat, solar absorptivity, and the coefficient of thermal expansion also affect temperature gradients and thermal response. The specific heat capacity of material is the quantity of heat required to increase the temperature of a unit mass of material by one degree. Solar absorptivity, or solar radiation, absorptivity is a measure of a material's ability to absorb solar radiation. The coefficient of thermal expansion is the change in unit length per degree of temperature change in a material. (Ghali, Favre, & Eldbadry, 2002)

Extensive research has been done on what factors affect thermal conductivity such as curing conditions, admixtures, concrete age, water to cement ratio, cement type, aggregate ratios, aggregate type and source, temperature, and humidity. The many contributing factors make an accurate prediction of a concrete's thermal conductivity a difficult task. Morabito's 1988 study measured the thermal conductivity of five different concrete mixtures and stated the most important factors influencing thermal properties of concrete are type of aggregate, type of cement, mix proportions, moisture content, and temperature. Morabito tested two lightweight concretes, a normal weight concrete, a heavy concrete, and a sand-mortar mixture. This study concluded that thermal conductivity increases with density and is independent of aggregate type in lightweight and normal weight concrete. In high-density concrete, aggregate type showed

some effects. For example, the barite aggregates used seemed to decrease the thermal conductivity from the expected value given the density. Additionally, Morabito concluded that thermal conductivity and thermal diffusivity decrease as temperature increases and thermal conductivity is higher in moist concrete. The lowest and highest thermal conductivity measured in the concrete mixtures was approximately 1.8 W/m-K and 2.8 W/m-K, respectively. A lower thermal conductivity of 1.2 W/m-K was measured in the sand-mortar mixture.

A 2003 study by KH Kim, Jeon, JK Kim, and Yang sought to formulate an accurate thermal conductivity prediction model. The thermal conductivity of twenty-two concrete and mortar specimens were tested using varying mix designs, curing conditions, age, aggregate source, temperature, and humidity. Researchers concluded that aggregate volume fraction and moisture condition had the greatest effect on thermal conductivity. This study also observed the same trend of decreasing thermal conductivity with increasing temperature. The lowest and highest thermal conductivities measured in the concrete mixtures was approximately 0.8 W/m-K and 2.5 W/m-K, respectively. A lower thermal conductivity of 0.7 W/m-K was measured in the mortar mixture.

Other design and reference materials give ranges of several thermal properties to be used by engineers. The American Society of Heating, Refrigerating, and Air-Conditioning Engineers (ASHRAE) 2009 Handbook states that, for normal weight concrete, thermal conductivity should be taken as 1.0-2.8 W/m-K. *Concrete Structures: Stresses and Deformation* (Ghali et al., 2002) gives the following thermal properties:

- Specific Heat: 840 – 1200 J/kg-^{o}C
- Thermal Conductivity: 1.5 – 2.5 W/m-K
- Solar Absorptivity Coefficient: 0.65 – 0.80

Concrete: Microstructure, Properties, and Materials by Mehta & Monteiro (2006) includes a discussion on the thermal properties of concrete including the coefficient of thermal expansion, specific heat, thermal conductivity, and thermal diffusivity. Mehta & Monteiro state that using common rocks and minerals, the coefficient of thermal expansion is lowest in concretes with limestone and gabbro, and highest in those containing sandstones, natural gravels, and quartzite. The authors state that the coefficient of thermal expansion can be accurately estimated from the weighted average of different types of rocks (assuming 70-80 percent aggregate in a concrete mixture). They also state that specific heat is not greatly affected by type of aggregate, temperature, or other parameters. Similarly to coefficient of thermal expansion, thermal conductivity is also affected by the mineralogical makeup of a concrete's aggregates, with the lowest conductivities observed in mixes containing basalt, and the highest in those with quartzite. Finally, thermal diffusivity is a property that is a function of thermal conductivity, specific heat, and density. Thermal diffusivity is another measure of how readily heat will move through a concrete and is mainly affected by thermal conductivity. Therefore, it is also affected by aggregate type. The typical ranges of values for thermal properties given by Mehta & Monteiro are:

- Coefficient of thermal expansion: $5 \times 10^{-6} – 11 \times 10^{-6}$ per ^{o}C
- Specific Heat: 900 – 1000 J/kg-^{o}C
- Thermal Conductivity: 1.9 – 3.5 W/m-K
- Thermal Diffusivity: 0.032 – 0.058 ft^2/hr

Regarding the coefficient of thermal expansion, *Design of Concrete Structures* by Nilson, Darwin, & Dolan (2004) agree that aggregate type is the major determining factor. In this text, it is stated that the coefficient of thermal expansion generally ranges between 7.2×10^{-6} per ^{o}C and

12.6 x 10^{-6} per ^{o}C with a value of 10 x 10^{-6} per ^{o}C being generally accepted as adequate for design of concrete structures.

The American Concrete Institute (ACI) publishes ACI 122R: Guide to Thermal Properties of Concrete and Masonry Systems. In this document, ACI again notes that thermal conductivity is most dependent on aggregate type but notes that this is a very difficult factor to quantify. Instead, thermal conductivity is often related to concrete density (ρ) for design. In a 1980 study by Valore, thermal conductivity is plotted as a function of oven-dry density:

$$k_c = 0.5e^{0.02\rho} \quad \textbf{(2.1)}$$

Where k_c is thermal conductivity in Btu-in/hr-ft^2 ^{o}F and ρ is oven-dry density in lbs/ft^3 or:

$$k_c = 0.072e^{0.00125d} \quad \textbf{(2.2)}$$

Where k_c is thermal conductivity in W/m-K and ρ is oven dry density in kg/m^3. However, concrete is rarely found in a completely moisture free environment and other studies have concluded that moisture content has an effect on thermal conductivity. Therefore, for concrete in normal air-dry conditions (not known to be exposed to high moisture) Valore recommends the following modified equations:

$$k_c = 0.6e^{0.02\rho} \quad \text{(U.S. Units)} \quad \textbf{(2.3)}$$

$$k_c = 0.0865e^{0.00125\rho} \quad \text{(S.I. Units)} \quad \textbf{(2.4)}$$

The original equations for the thermal conductivity of oven dried concretes are included in ACI 122R but it is noted that thermal conductivity can still differ among concretes with the same density. Using this equation, normal weight concrete (130-150 lb/ft^3) has a thermal conductivity range of 1.0 - 1.45 W/m-K.

As part of the research conducted by Lee in 2010, researchers studied how temperature gradients were impacted by varying three thermal properties: thermal conductivity, specific heat, and solar absorptivity. In the 2D finite element model used in this study, thermal conductivity

varied between 1.5 and 2.5 W/m-K, specific heat was varied between 800 and 1200 J/kg ^{o}C, and the solar absorptivity coefficient was varied between 0.5 and 0.8. Lee concluded that by varying these factors, the temperature at an individual point was only affected up to 5% and negligible effects were seen on the overall temperature gradients.

Despite the fact that there are many factors contributing to the various thermal properties of a concrete mixture, the ranges of potential values for these properties are not large enough to impact temperature gradients. It is safe to assume that even though different mixtures from different sources are used in this study, values will not fall outside the typical values found in past research and reference materials. Typical values, specified in Section 4.3, will be used for the modeling portion of this research.

2.2. Temperature Gradients in Bridge Structures

Early research in 1978, conducted by Yargicoglu and Johnson, concluded that temperature gradients increased the compression and tension stresses in bridges during different times of the year. In one instance, for the bridges monitored in Austin, Texas, the temperature induced stresses alone reached approximately 80% of the AASHTO cracking stress. Around the same time, Priestley was working to develop a model to represent temperature distribution and quantify the resulting stresses in New Zealand. Priestley determined that the major source of heat input was solar radiation on the top surface of the bridge girder. For the box girder section examined, Priestley stated that transverse heat flow was insignificant when compared to the vertical heat flow. Therefore, a vertical thermal gradient was developed based on one-way heat flow analyses (Priestley, 1976). Priestley proposed a fifth-order curve for the vertical temperature gradient and determined that thermal response was influenced by three major factors: (1) greater wind speeds decreased the magnitude of temperature differences; (2) days

with the greatest ambient air temperature range produced the greatest temperature differences in the box girders; and (3) black top, or bridge deck thickness affected thermal response. Priestley's proposed gradient developed from his work on box girders is still widely used today. The Priestley Model is depicted in Figure 2.1.

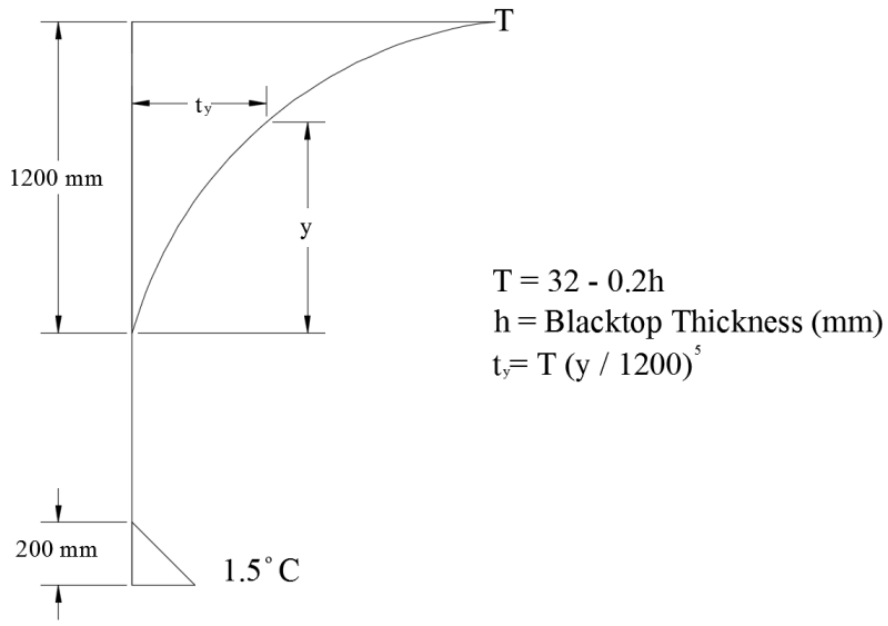

Figure 2.1 - Priestley proposed vertical temperature gradient (Priestley, 1976)

In the United States, Potgieter and Gamble (1983) completed a similar study to Priestley's. They also proposed a fifth-order curve to describe the vertical temperature distribution in bridge girders and verified their results with field data from the Kishwaukee Bridge in Illinois. Their research was mostly in agreement with Priestley's conclusions. Due to the wide variations of climatic conditions in the United States, Potgieter and Gamble recommended that location be considered when determining temperature distributions. Furthermore, Potgieter and Gamble developed specific equations to estimate thermal stresses for T-beams, rectangular girders, and box girder sections. These equations were meant to simplify the design process. In addition, they stated that proper placement of deformed bar reinforcement

was sufficient to account for temperature induced stresses. Finally, they recommended that AASHTO design standards be modified to include thermal response based on location, type of section, surface condition, and bridge alignment (Potgieter & Gamble, 1983). In 2002, an observational study verified that the Potgieter and Gamble equations, and therefore the Priestley Model, were both accurate in predicting temperature gradients for a box girder in San Antonio, Texas (Roberts-Wollman, Breen, & Cawrse, 2002).

In 1989, AASHTO published specifications for thermal effects in concrete bridge superstructures, the first American design standard including temperature gradients (AASHTO, 1989). The vertical temperature gradient proposed in this document was a result of The National Cooperative Highway Research Program (NCHRP) Report 276, completed by Imbsen et al. in 1985 and is shown in Figure 2.3 (Roberts-Wollman et al., 2002; AAHSTO, 1989; Imbsen, Vandershaf, Schamber, & Nutt, 1985). Priestley's work, as well as Potgieter and Gamble's, contributed to the NCHRP report. The 1989 AASHTO model split the United States into four regions based on solar radiation, shown in Figure 2.2. The AASHTO 1989 model used three straight lines instead of the fifth-order curve used in previous gradients. The magnitude of these lines depended on the solar radiation zones shown in Figure 2.2. In 2007, AASHTO simplified the model further by using only two straight lines in the top section of the girder (AASHTO, 2007). The current AASHTO design model, established in 2012, is only a slight modification from the 2007 model. The AASHTO 2012 model uses two straight lines for the top sections, one straight line for the bottom, and is based on the same four solar radiation zones that were originally established in 1989 (AASHTO, 2012). The design temperature gradient remained unchanged in the 7th edition released in 2014 (AASHTO, 2014). The current positive gradient is displayed in Figure 2.4. The AASHTO specifications also state that a negative temperature

gradient can be obtained by multiplying the location-specific positive values by -0.30 for concrete decks or -0.20 for asphalt decks. In Figure 2.4, if the overall depth is 16 inches or more, the *A* dimension should be taken as 12 inches. If the overall depth is less than 16 inches, the *A* dimension should be taken as the actual depth minus 4 inches. The specifications also state that the bottom temperature should be taken as 0°F unless a specific study warrants a different value, but 5°F should be treated as a maximum.

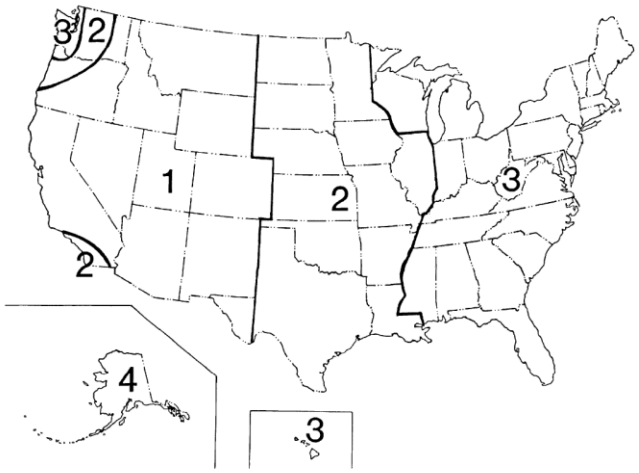

Figure 2.2 – AASHTO Solar Radiation Zones (AASHTO 2014)

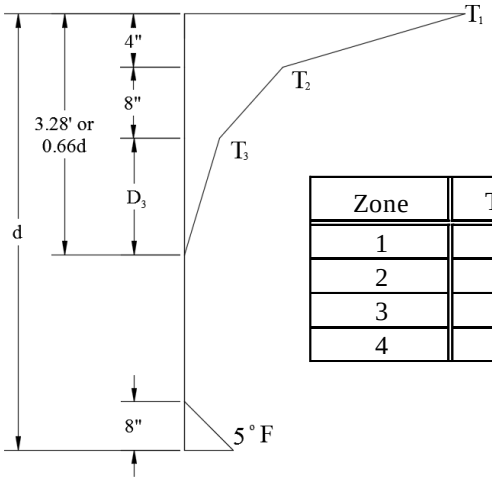

Zone	T_1 (°F)	T_2 (°F)	T_3 (°F)
1	54	14	5
2	46	12	4
3	41	11	4
4	38	9	3

Figure 2.3 - 1989 AASHTO Vertical Design Gradient (AASHTO 1989)

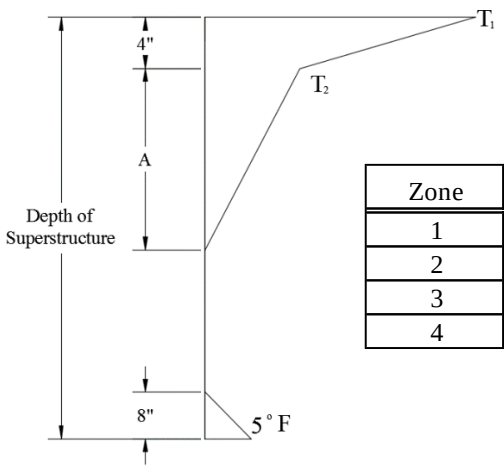

Zone	T_1 (^oF)	T_2 (^oF)
1	54	14
2	46	12
3	41	11
4	38	9

Figure 2.4 - 2014 AASHTO Vertical Design Gradient (AASHTO 2014)

It is important to again note that because the AASHTO model is based on Imbsen's work (and therefore Priestley, and Potgieter and Gamble), the thermal response of a section considers solar radiation from the top surface as the main heat-contributing source and is based on a one-way heat flow model. Currently, no transverse temperature gradient is included in the AASHTO LRFD Bridge Design specifications.

Additional research on this subject is extensive. In 2005, Barr, Stanton, and Eberhard analyzed the effects of high fabrication temperatures on initial camber and prestressing strand stress. More pertinent to this study, it was determined that by applying the appropriate design temperature gradients, bottom stress in girders could reach 60% of the allowable stress from temperature effects alone. Nguyen, Stanton, Eberhard, and Chapman completed a study in 2015 researching how daily variations in temperature profile affected the camber of bridge girders and developed a model to predict this. Hoffman, McClure, and West (1980) conducted field measurement of box girders in Pennsylvania and compared results to available models at the time. Mirambell and Aguado (1990) evaluated the response of multi-cell box girders and determined that among geometrical parameters, depth, and ratio of top and bottom portions to

each other have the greatest influence on thermal response. Saetta, Scotta, and Vitaliani (1995) presented a numerical method to predict thermal response that agreed with the previously mentioned work on box girders. Kennedy and Soliman also developed a specific model for steel and concrete composite bridges in 1987. Two studies performed on the Confederation Bridge in Canada sought to assess the validity of current models to the deep members used in that bridge. Confederation Bridge girders were up to 45 feet deep and 36 feet wide. It was determined that the AASHTO and Priestley models were inaccurate for members of this size and a specific temperature gradient was proposed by researchers (Gilliland & Dilger, 1997; Li, Maes, & Dilger, 2004). The Calgary Model proposed for the largest girders in the Confederation Bridge is depicted in Figure 2.5.

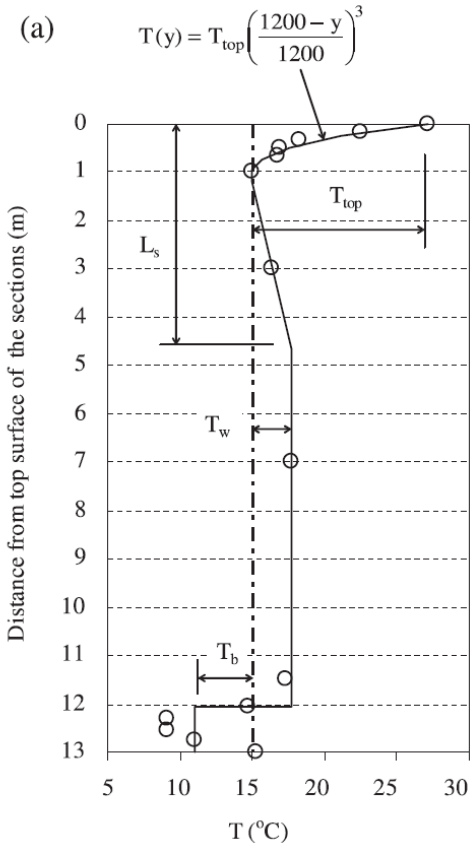

Figure 2.5 - Calgary Model from Confederation Bridge (Li et al., 2004)

Researchers at the Georgia Institute of Technology suggested that the current AASHTO model is inaccurate at predicting temperature distributions in many girder shapes, specifically I-beams (Hurff, 2010; Lee, 2011; Lee, 2010). Lee conducted a study in 2010 that monitored an AASHTO PCEF-63 girder in Atlanta, Georgia. He considered solar radiation on all surfaces of the girder exposed to sunlight and developed a two-way heat flow model using finite element analysis. This method allowed researchers to analyze the effect of two-way heat transfer on the vertical gradient, as well as develop a transverse design gradient. The gradients based on this method were in good agreement with the measured temperatures in their test specimen, a BT-63 bulb tee section. Among other conclusions, Lee's research indicated that neither girder orientation nor wind speed had a significant effect on vertical gradients. An East-West orientation produced the largest vertical and transverse gradients, but the difference was more pronounced in the transverse gradients. While Lee only experimentally monitored one girder section, the modeling portion of his study found that among the four AASHTO sections studied, the Type V and BT-63 experienced the largest temperature gradients. Ultimately, Lee's research concluded that the AASHTO model underestimated the thermal gradient in I-beams and recommended that it should be revised. If thermal gradients are underestimated, the corresponding thermal stresses will also be underestimated leading to durability, serviceability, and stability concerns. The recommended vertical gradient from this research work is shown in Figure 2.6 and the recommended transverse gradients in Figure 2.7.

It can be observed from this review that the most cited research in this field has been conducted on girder sections with wide top flanges and design gradients established on one-way vertical heat flow. Even the AASHTO LRFD Bridge Design Specification thermal design gradient is based on these conditions. It has been determined that this design gradient is not

applicable to all shapes such as unusually deep sections (Li et al., 2004). It is not been experimentally verified whether the AASHTO design gradient is applicable to bulb-tee sections with top flanges that are not wider than the base. Recent research has also determined that two-way heat flow is also a more accurate method at predicting temperature gradients (Lee, 20100. This will be of particular concern for I-sections without large upper flanges casting shade on the lower portion of the beam. Bulb-tee sections are very common on highway bridges in the United States and therefore understanding the specific temperature gradients in these sections is an important topic.

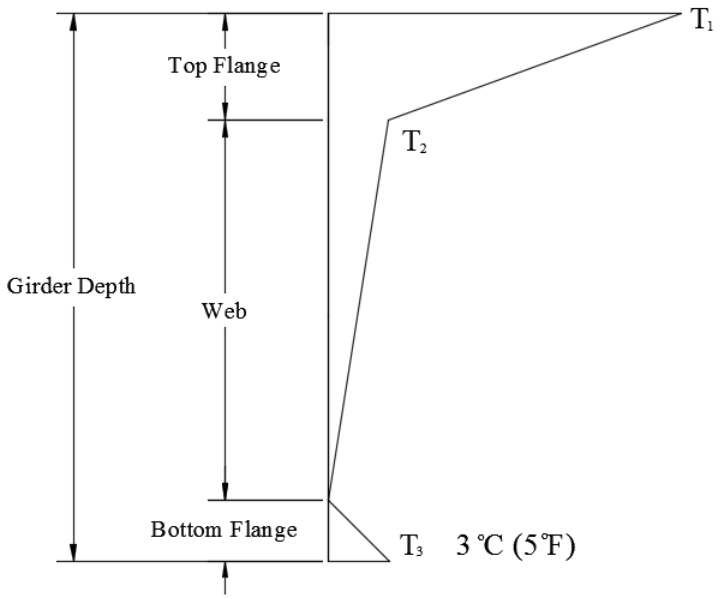

City	Vertical Differential, °C (°F)	
	T_1	T_2
Alamosa, CO	30 (54)	7.2 (13)
Phoenix, AZ	29 (52)	6.7 (12)
Medford, OR	29 (52)	5.6 (10)
Atlanta, GA	27 (48)	6.1 (11)
Brownsville, TX	26 (46)	6.7 (12)
Caribou, ME	26 (46)	5.0 (9)
Hilo, HI	26 (46)	6.7 (12)
Annette, AK	23 (42)	4.4 (8)

Figure 2.6 - Lee Vertical Temperature Gradient (Lee, 2011)

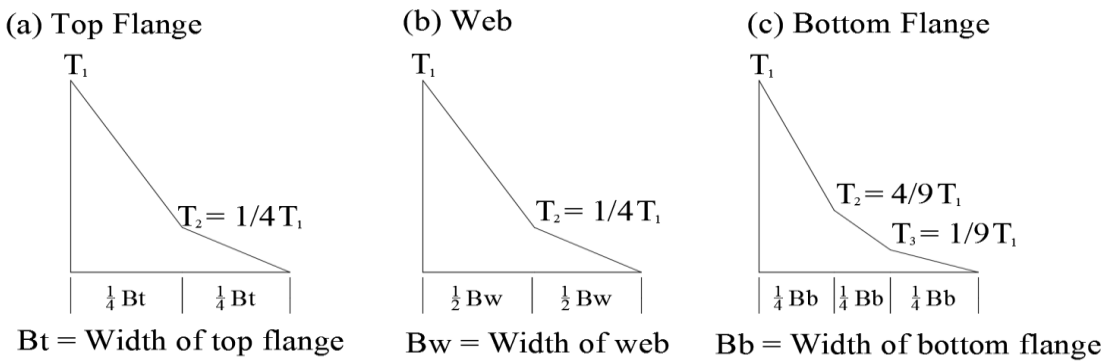

City	Transverse Differential, T_1, °C (°F)		
	Top Flange	Web	Bottom Flange
Alamosa, CO	24 (43)	18 (32)	30 (53)
Phoenix, AZ	20 (36)	16 (29)	26 (46)
Medford, OR	18 (32)	14 (25)	22(40)
Atlanta, GA	19 (35)	15 (27)	25 (45)
Brownsville, TX	18 (32)	14 (25)	24 (43)
Caribou, ME	20 (36)	16 (29)	25 (45)
Hilo, HI	16 (29)	14 (25)	23 (41)
Annette, AK	13 (23)	10 (18)	15 (27)

Figure 2.7 - Lee Transverse Temperature Gradients (Lee, 2011)

3. Methods and Materials

3.1. Fabrication

In this study, five full scale AASHTO bridge girder segments were cast and their temperatures were monitored. Reusable wooden formwork to construct segments four feet in length were built at the University of Arkansas Engineering Research Center (ERC) in Fayetteville, Arkansas. Beams were cast using local materials in Fayetteville and Norman, Oklahoma. In Norman, one AASHTO Type II section and one AASHTO Type IV section were cast. In Fayetteville, one AASHTO Type II, and one AASHTO Type IV were cast. Additionally, midway through the experiment, an AASHTO Type V section was also cast in Fayetteville so that results could be compared to previous research on sections of similar size.

3.1.1. Concrete Mixtures and Placement

In Fayetteville, concrete was mixed and placed on site at the ERC for the Type II and Type IV sections. For the Type V, concrete was donated by GCC Ready Mix. GCC mixed the concrete, then transported it to the ERC to be placed. In Norman, concrete was donated by Dolese Bros. Company. Dolese Bros. prepared the concrete at their ready mix plant and then transported it to Fears Structural Laboratory on the University of Oklahoma's campus where it was placed. The mix designs from each source are listed in Table 3.1, the concrete mixed on site at the ERC in Fayetteville, AR is denoted as "Fayetteville." The mix provided by Dolese Bros. had a slump of six inches. The mix provided by GCC had a slump of four inches. The mix prepared on site at the ERC was a self-consolidating mix. The sections were not prestressed as prestressing steel should have no effect on the temperature distribution. The construction process for all three sections is shown in Figure 3.1.

Table 3.1 – Concrete mix proportions

	Dolese Bros. [lb/yd^3]	GCC [lb/yd^3]	Fayetteville [lb/yd^3]
Cement	414	416	775
Fly Ash	103	104	-
Water	167	250	275
Coarse Aggregate	1857	1650	1410
Fine Aggregate	1516	1445	1520
Water Reducer	42 oz	- oz	54 oz
w/cm Ratio	0.32	0.48	0.35

Figure 3.1 – Girder segment construction process

3.2. Instrumentation

3.2.1. Temperature Measurement

Before each beam was cast, thermocouples were placed at 12 locations throughout the cross section at the midpoint of the segment. After the beams set, thermocouples were also placed at 17 external surface locations. The distribution of measurement locations was chosen to provide a comprehensive picture of temperature gradients in both the vertical and transverse direction. The thermocouple locations are shown in Figure 3.2.

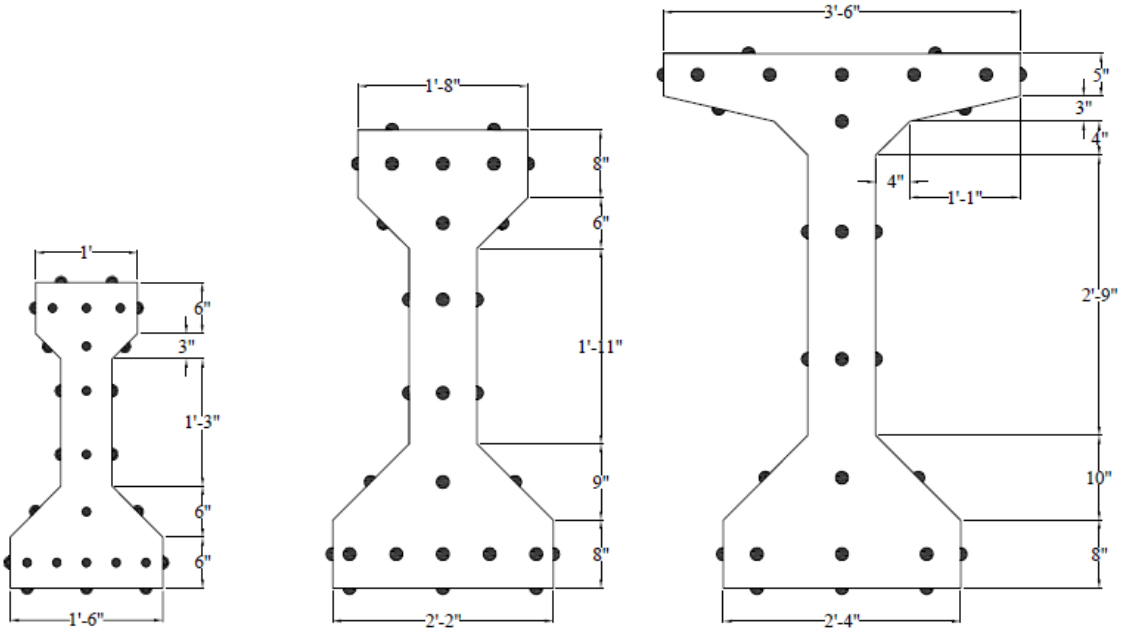

(a) (b) (c)

Figure 3.2 - Thermocouple locations for (a) Type II, (b) Type VI, and (c) Type V

Type T thermocouple wire was used to measure temperature at all locations. For the internal thermocouples, bare lead probes were coated in a Sikadur epoxy to prevent water from causing the probes to malfunction. Sikadur epoxy has a high thermal conductivity and does not act as an insulator. The thermocouples were then attached to a minimal frame of reinforcing steel to be placed into the forms. Enough steel was used to account for any potential temperature and

shrinkage cracking as well as provide a frame to hold the thermocouples in their desired locations. The thermocouples were placed so that there was no contact between the actual probe and the steel to avoid any influence on the temperature readings. For the internal thermocouples, two probes were placed at each location to provide a backup option in the event that any issues were encountered. In Figure 3.3, the bottom row of internal thermocouples for the Arkansas Type II are pictured attached to the steel frame, before placement in the formwork.

Figure 3.3 – Internal Type II thermocouples

Obtaining accurate surface temperature readings required several different methods. First, bare lead thermocouples were placed on the surface of the beam segments and held in place using an epoxy putty. Next, a test batch of washer thermocouples were epoxied to the concrete surface. Some probes were left uncovered, some covered with epoxy putty, and some covered with an insulating material. All of these methods seemingly failed to capture the true surface temperature of the concrete and instead were more influenced by the ambient air temperature. For the final method, small holes (1/8" diameter) were drilled approximately 0.5" into the concrete surface. Then, bare lead thermocouples were placed into these holes and epoxied in place. These thermocouples had a higher rate of failure than the internal locations presumably

because water entered the holes and caused a malfunction. It was believed this method would provide more accurate readings but this was not the case. These probes were still more influenced by ambient air temperature. There is a more detailed discussion on this issue in Section 4.1.1.

3.2.2. Strain Measurement

To confirm temperature measurements recorded by the thermocouples, detachable mechanical strain (DEMEC) points were placed on the face of two beam segments. Expansion readings were taken over the course of a particular day. This process was performed on the Type V and Type IV sections in Fayetteville, AR. Where space permitted, four point grids were placed on the faces of the south side of each girder. On the smaller faces, only two horizontal points were placed. Measurements were taken with an eight inch DEMEC gauge, pictured in Figure 3.4.

Figure 3.4 – Expansion/strain measurement with DEMEC gauge

The earliest reading in the morning was taken as zero expansion and then as the temperature rose and the girder heated, subsequent expansion readings were recorded. The percent strain was calculated using the known gauge length and measured change in distance between the points. Then, a coefficient of thermal expansion within the range of typical values

for concrete was used to estimate the approximate temperature rise from the measured expansion and compared to the measured temperature rise over that same time period. There are some inherent assumptions in this comparison, mainly that expansion readings on the surface of the beam were compared with internal temperatures. This assumes that the temperature is constant in the transverse direction which is not the case. However, this comparison still gives a good representation of whether the overall gradients are accurate and therefore served as a physical confirmation of the accuracy of the temperature collection process.

3.3. Experimental Test Set-Up

After all the thermocouples were placed for each segment, they were attached to data acquisition systems which recorded readings at ten minute intervals. In Fayetteville, AR, a Measurement Computing USB-2416 data acquisition board with expanded inputs collected data for each beam segment. Due to its capability, only two beams were monitored simultaneously at the Fayetteville test site. For the Measurement Computing multiplexers, data were recorded to a laptop. Data were uploaded at approximately two-week intervals. In Norman, OK, a Campbell Scientific data acquisition was used. The Type II beam was attached to a Campbell Scientific AM4 multiplexer and the Type IV was attached to an AM16/32 multiplexer. A CR10X data-logger recorded the data from each multiplexer. Data were uploaded at two-week intervals. Both systems ran continuously and were solar powered. There were some gaps in data collection due to maintenance or temporary loss of power. These data gaps did not affect the results or conclusions of this study. Sufficient data were still collected to provide an adequate picture of the thermal distribution in all beam sections. The Fayetteville data acquisition system is pictured in Figure 3.5 and the Norman system in Figure 3.6.

Figure 3.5 - Fayetteville Data Acquisition System – Measurement Computing USB-2416

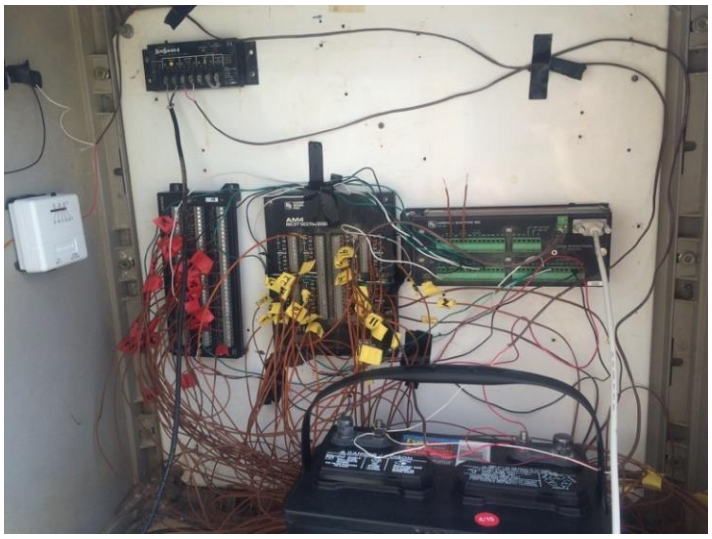

Figure 3.6 - Norman Data Acquisition System – Campbell Scientific AM4 and AM16/32 multiplexers with CR10X data logger

Shown in Figure 3.7 is a fully instrumented girder segment. Actual field conditions for bridge girders were imitated as best as possible. The girders were positioned off the ground to prevent any effects from the ground and to allow air to flow beneath them as would be the case on an actual bridge. A dark colored sheet was placed under each beam to prevent excess reflected solar radiation since the beams were so close to the ground. This also created a consistent surface beneath the segments between the two test sites. Between the masonry

supports and the beams, wood was placed because of its low thermal conductivity. Extruded polystyrene foam sheets were attached to the ends of each segment to prevent heat loss or gain through the ends, thus replicating a full-length girder. Finally, the lift hooks used to transport the beams were insulated to mitigate potential thermal affects. Surface thermocouples and the bundle of internal thermocouples exiting the beam can also be seen on Figure 3.7.

Figure 3.7 - Fully instrumented Type IV girder segment – Norman, OK

At both test sites, the girders were oriented spannng in the East-West direction. Previous research concluded this orientation produced the largest vertical and transverse temperature gradients (Potgieter & Gamble, 1983; Lee, 2010). Specifically, with only one side of the girders exposed to sunlight, this orientation should have the most effect on transverse gradients. The Arkansas test site (with the Type V and Type IV in place) is pictured in Figure 3.8 and the Oklahoma test site is pictured in Figure 3.9.

Environmental data were not collected directly at the test sites. Therefore, in order to analyze the environmental conditions which resulted in the most extreme temperature gradients, weather data were collected from nearby National Oceanic and Atmospheric Administration

(NOAA) stations. Data recorded from NOAA included maximum and minimum daily temperatures, average daily wind speeds, and precipitation. Surface solar radiation readings were also collected from weather stations which was used for modeling and comparison purposes. The Drake Field station was used in Fayetteville, which is approximately 2.5 miles from the actual test site. A combination of local weather stations in Norman, OK were used to obtain full coverage and an accurate representation.

Figure 3.8 - Fayetteville, AR test site (Type V and Type IV)

Figure 3.9 - Norman, OK test site (Type II and Type IV)

3.4. Modeling Temperature Distribution

A finite element modeling program, HACON, was used to predict the thermal gradients experienced in different concrete cross sections. HACON was originally developed to model the temperature and stress development in hardening concrete. By tailoring the input, this program was a useful tool to apply solar radiation to the exposed surfaces of bridge girders and model heat flow. As previously noted, solar radiation is the main component in determining vertical and transverse temperature gradients. Solar radiation on a horizontal surface was predicted using the following method, Equations 3.1-3.4, from Thepchatri, Johnson, and Matlock (1977) and Cooper (1969).

$$I(t) = \frac{1.7S}{T}\left(\frac{sin^2\alpha + 2sin^2\alpha}{3}\right) \quad \textbf{(3.1)}$$

I(t): solar insolation at time t of day on horizontal surface

S: total daily solar insolation

T: length of day (hours of sunlight)

$$\alpha = 90 - \Phi + \delta \quad \textbf{(3.2)}$$

Φ: latitude of location

$$\delta = 23.45 \sin\left(\frac{360(284+n)}{365}\right) \quad \textbf{(3.3)}$$

δ: declination angle of sun

n: day number of the year

The solar radiation on an inclined surface can then be adjusted using the following relationship:

$$I(t) = \frac{\sin(\alpha+\beta)}{sin\alpha} \quad \textbf{(3.4)}$$

β: angle on inclined surface

The total daily solar insolation or radiation is dependent on the time of year and location. While there are several available methods and resources to obtain this information, the National

Renewable Energy Laboratory (NREL) possesses the most comprehensive. In their manual, "Solar Radiation Data Manual for Buildings," (1995) NREL reports values such as the average incident solar radiation per day, average climatic conditions (temperature ranges, record maximum, record minimum, etc.), and average incident illuminance. For this research, the clear-day global average incident solar radiation per day was needed to predict the solar radiation experienced by the bridge girders. Limited by the locations chosen by NREL, Fort Smith, AR was chosen to represent Fayetteville, AR, and Oklahoma City, OK was chosen for Norman, OK. The average solar radiation per day for these locations is summarized in Table 3.2.

Table 3.2 - Clear-day global average incident solar radiation on a horizontal surface

	Arkansas	Oklahoma
	[Btu/ft^2/day]	[Btu/ft^2/day]
January	1110	1110
February	1450	1450
March	1890	1900
April	2310	2320
May	2550	2570
June	2630	2650
July	2560	2590
August	2330	2360
September	1970	2000
October	1540	1550
November	1150	1160
December	1000	1000

This provided the necessary information to calculate the solar radiation on each exposed surface of the bridge girders. The shade of the top flanges was also taken into account during this process. While solar radiation was not directly measured at the test sites, this method produced good agreement with the nearest stations measuring solar radiation in both Fayetteville, AR and

Norman, OK. These predicted solar radiation values were then applied to the corresponding surfaces in the HACON modeling program. Models were run over a multi-day period in an attempt to account for any retained heat that could have effects on the measured thermal gradients. On the final day of each simulation, maximum vertical and transverse temperature gradients were recorded and compared with the measured gradients at the corresponding location and time.

3.5. Quantifying Stress

Two dimensional internal self-equilibrating stresses from vertical and transverse temperature gradients were quantified using the method outlined in *Concrete Structures: Stresses and Deformation* (Ghali et al., 2002). This method is summarized and simplified below in Equations 3.5-3.6. Self-equilibrating stresses, or longitudinal stresses, occur in statically determinate bridge structures when the temperature gradient is non-linear, as is the case in optimized bridge girder sections. Continuity stresses only occur from temperature gradients if displacements and rotations at member ends are restrained, known as an indeterminate structure. For the purpose of this study, beam segments will be taken as simple-span, determinate sections, where rotation at the member ends is free to occur. To begin, concrete expands or contracts with temperature increase or decrease. The strain that would result from a temperature rise at a point *y* from the centroid of the beam is a function of the coefficient of thermal expansion and temperature. The stress required to restrain this strain is:

$$\sigma_T = -E\alpha_t T(y) \qquad \textbf{(3.5)}$$

E: modulus of elasticity

α_t : coefficient of thermal expansion

T(y): temperature rise at any point at a distance y below centroid

This stress will result in a constant axial force (F) and bending moment (M) throughout the beam acting at the centroid of the section.

$$F = \int \sigma_T dA \quad \textbf{(3.6)}$$

$$M = \int \sigma_T y dA \quad \textbf{(3.7)}$$

The stress at any fiber can then be represented by simply adding the stress due to the axial force (σ_F) and bending moment (σ_M) from the stress that would be produced by the temperature gradient (σ_T). Figure 3.10 displays this process in a simple beam with an arbitrary vertical thermal gradient.

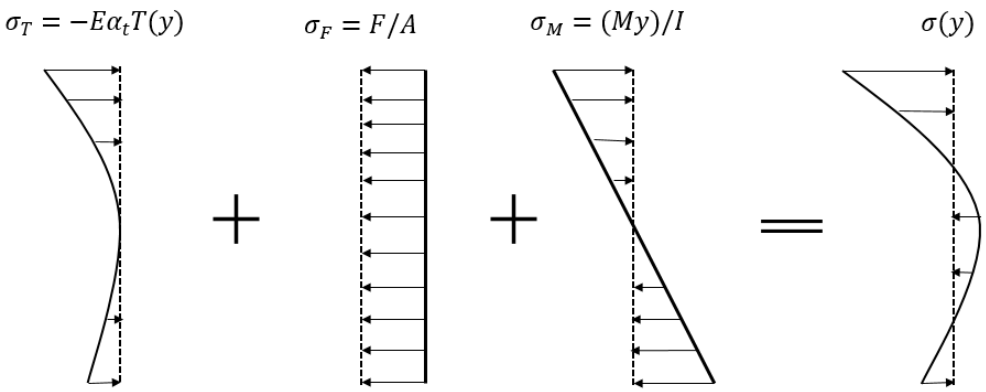

Figure 3.10 – Theoretical Stress Profiles

The method outlined above allows a known temperature gradient to be applied to any given section and results in internal stress as a function of location in the cross section. Girders were then modeled in SAP2000 to verify this method. By neglecting the self-weight and using a simply supported beam, the maximum compressive and tensile stresses from a non-linear vertical temperature gradient were confirmed in SAP2000. Verification of this method allowed conditions to then be modified within SAP2000 to further investigate the three dimensional response of girders under more accurate conditions such as including the effects of self-weight,

bearing on elastomeric bearing pads, the presence of prestressing strands, and combined vertical and transverse temperature gradients. The results of these calculations can be found in Section 4.5.

4. Results and Discussion

4.1. Measured Temperature Gradients

4.1.1. Vertical Gradients

Temperature readings were collected at ten minute intervals continuously for nine months. Table 4.1 displays the maximum vertical gradients observed in each beam for each month of the temperature collection process. Maximum vertical gradients were calculated as the difference between the highest and lowest readings in the center vertical line of thermocouples. Generally, the daily maximum vertical gradient was observed near the time of maximum solar radiation, approximately 2:00pm. The majority of the most extreme vertical gradients were also observed at the Arkansas location, rather than the Oklahoma site. This is most likely because of the difference in environmental conditions. The test site in Arkansas did not experience as consistently warm temperatures as the Oklahoma site, but generally had lower wind speeds and greater ambient temperature variations over the course of a day. Based on previous research, these conditions are known to increase the severity of temperature gradients (Priestley, 1976; Potgieter & Gamble, 1983; Lee, 2010). This also suggests extreme heat does not necessarily produce the most extreme temperature gradients.

The Type V section in this study only had consistent data for September, October, and November. As was previously stated, the Type V section was cast midway through this project as a way to compare data with similar studies and therefore has no data for the first part of the study. Some issues were encountered in the last months of 2015 supplying power to the Arkansas data acquisition system, so consistent data was not able to be collected for the months of December and January. Vertical temperature gradients are not maximized during these months, so the missing data does not affect any results or analysis.

Table 4.1 - Maximum measured vertical temperature gradients

Month	Section	Location	Date	Time	Vertical Gradient [°C / °F]	
May '15	**II**	**AR**	**18-May**	**3:00pm**	**25.8**	**46.5**
	IV	AR	18-May	2:00pm	25.2	45.4
	V	-	-	-	-	-
June '15	II	AR	28-Jun	2:15pm	24.1	43.4
	IV	**AR**	**29-Jun**	**2:00pm**	**26.0**	**46.8**
	V	-	-	-	-	-
July '15	II	AR	4-Jul	2:10pm	22.7	40.9
	IV	AR	4-Jul	2:10pm	23.1	41.5
	V	-	-	-	-	-
August '15	II	AR	20-Aug	1:15pm	24.7	44.5
	IV	AR	28-Aug	3:00pm	21.7	39.0
	V	-	-	-	-	-
September '15	II	OK	22-Sep	5:20pm	13.6	24.5
	IV	AR	21-Sep	1:50pm	22.4	40.3
	V	AR	21-Sep	1:00pm	37.3	67.2
October '15	II	OK	14-Oct	1:50pm	12.2	22.0
	IV	AR	14-Oct	2:00pm	23.9	43.1
	V	**AR**	**14-Oct**	**12:45pm**	**40.2**	**72.3**
November '15	II	OK	1-Nov	2:00pm	11.7	21.0
	IV	OK	1-Nov	1:00pm	8.9	16.0
	V	AR	23-Nov	12:00pm	36.9	66.5
December '15	II	OK	3-Dec	1:20pm	10.0	18.0
	IV	OK	9-Dec	1:30pm	8.6	15.5
	V	-	-	-	-	-
January '16	II	OK	12-Jan	1:20pm	10.4	18.8
	IV	OK	28-Jan	1:00pm	9.2	16.6
	V	-	-	-	-	-

The Type II maximum vertical gradient was observed on May 18 at 3:00pm, the Type IV on June 29 at 2:00pm, and the Type V on October 14 at 12:45pm. The measured temperatures for these times are displayed below in Figure 4.1, Figure 4.2, and Figure 4.3.

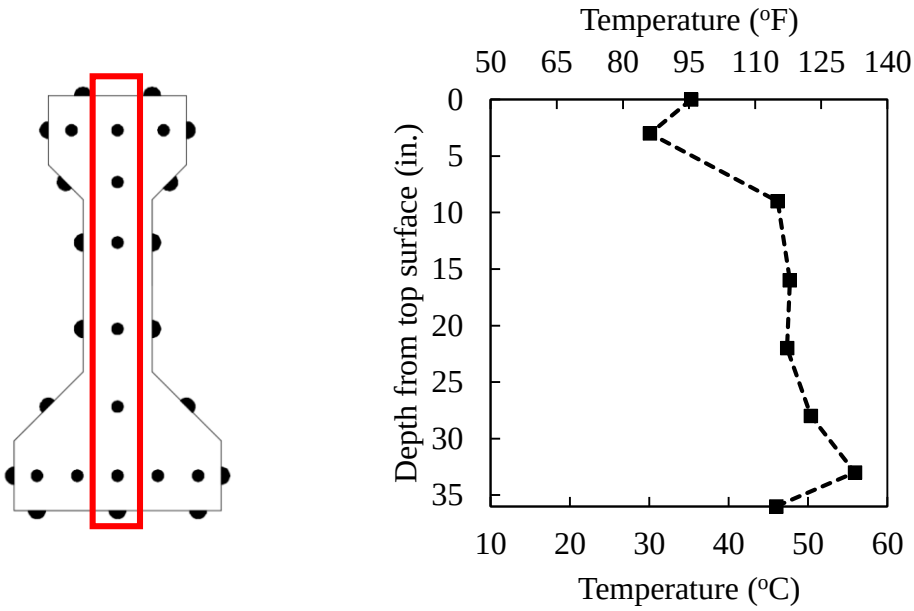

Figure 4.1 - Type II maximum vertical gradient - May 18, 3:00pm, Fayetteville, AR

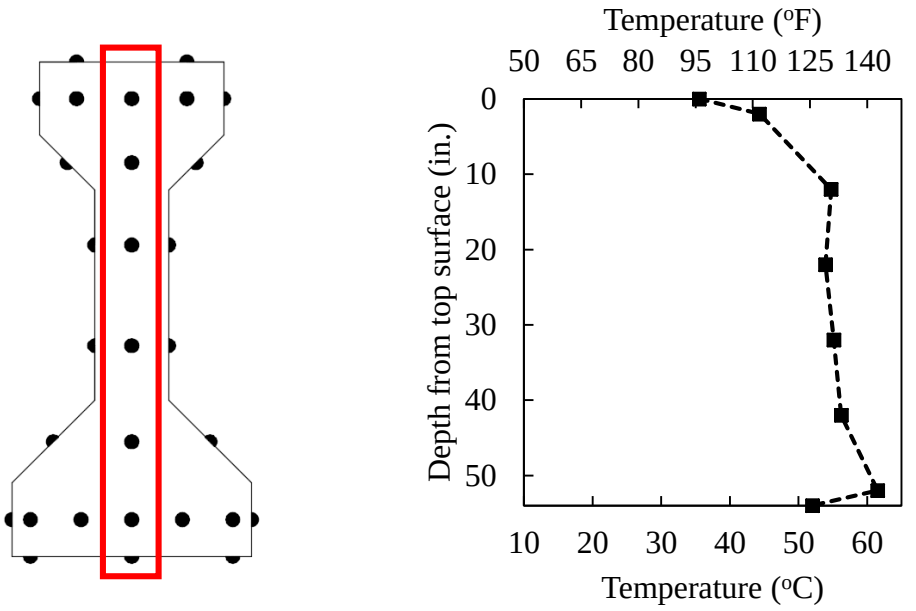

Figure 4.2 - Type IV maximum vertical gradient - June 29, 2:00pm, Fayetteville, AR

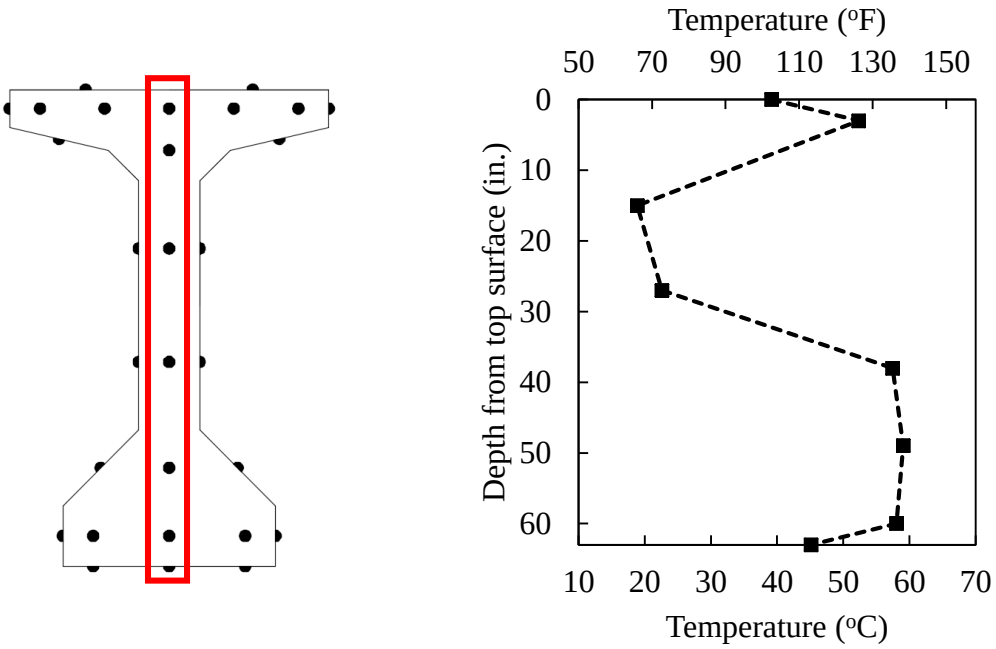

Figure 4.3 - Type V maximum vertical gradient - October 14, 12:45pm, Fayetteville, AR

All three of these figures display that despite several attempts, the surface thermocouples still did not capture the actual surface temperature. In all but one case, they seem to fall outside the temperature trend suggesting that they were more influenced by the ambient air temperature than the temperature of the concrete. While there are possible explanations for this, such as the surface of the girder not retaining as much heat as the interior of the girder, it is more likely that these probes were not accurate at reading surface temperatures and that the internal thermocouples display a more accurate picture of the temperature distributions in the girders. Figure 4.4 displays the measured temperature changes in a washer thermocouple, a bare lead thermocouple in a drilled hole, and an internal thermocouple compared with the ambient air temperature on October 12, 2015 in Fayetteville, AR. Both external thermocouples were on a surface exposed to direct sunlight yet their temperature variations mirror the ambient air temperature almost exactly. The external thermocouples also show more noise than the internal

reading. The data in Figure 4.4 suggests that both external thermocouples were recording air temperature instead of surface temperature.

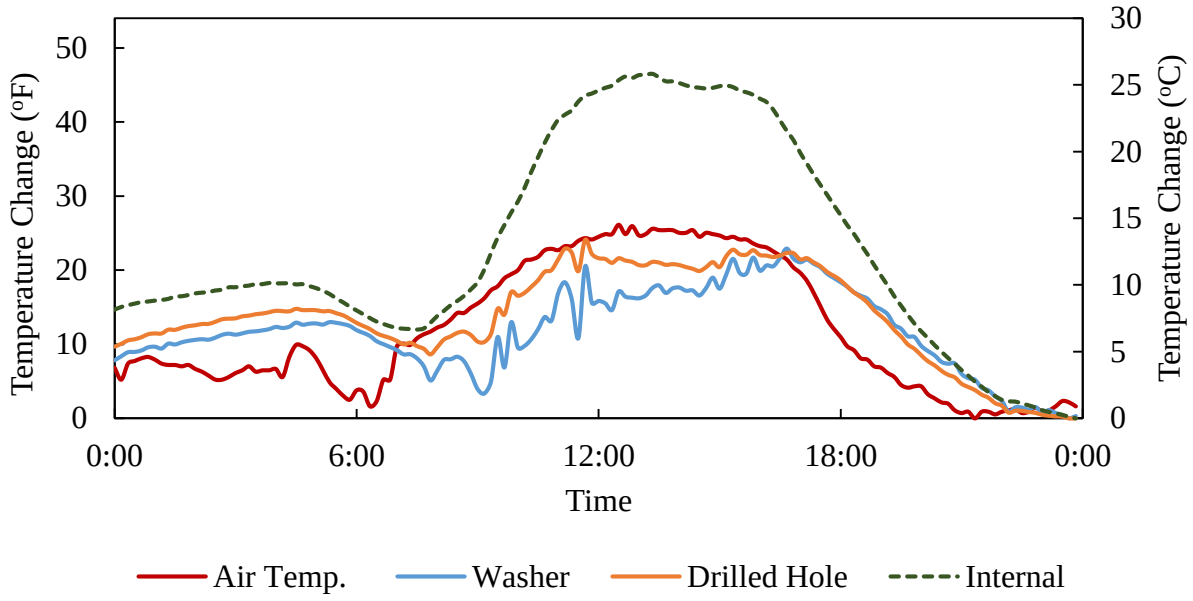

Figure 4.4 – External thermocouple comparison in top flange

There is a distinct difference between the vertical gradient measured in the Type V section with those measured in the Type II and IV. The smaller sections display similar gradients while the Type V has much higher temperatures in the top flange as well as lower temperatures in the upper web. This is most likely due to the differences in girder geometry. The Type II and IV sections have relatively small upper flanges that do not absorb as much solar radiation as the large top surface of the Type V. The wide upper flange of the Type V also casts a larger shadow on the lower portion of the girder. The effect of this shading can be seen clearly in the Figure 4.3.

One of the initial goals of this study was to examine how extreme heat events affect thermal gradients. To do this, Table 4.2 displays a summary of the environmental conditions on the days when the maximum gradients were observed. As all maximum gradients were observed in Fayetteville, AR, the environmental conditions displayed in Table 4.2 are for the Arkansas test site.

Table 4.2 – Environmental conditions on days of maximum observed vertical gradients

Site	Date	Max. Temp	Min. Temp	Temp Change	Max. Temp	Min. Temp	Temp. Change	Precip.	Avg. Wind	
		[°F]	[°F]	[°F]	[°C]	[°C]	[°C]	[in.]	[m/s]	[mph]
AR	18-May	83.0	56.0	27.0	28.3	13.3	15.0	0.0	0.9	2.0
AR	29-Jun	85.0	66.0	19.0	29.4	18.9	10.6	0.0	3.0	6.7
AR	14-Oct	87.0	42.0	45.0	30.6	5.6	25.0	0.0	0.5	1.1

All three of these days had relatively high temperature differences and low wind speeds with no precipitation. For comparison, the average daily temperature difference for May and June was 20°F (11°C), and was 26°F (14°C) for October 2015. All three of the days in Table 4.2 fell near or above these averages. Specifically on October 14th, there was a large variation in temperature. While the overall maximum vertical gradients were not observed on this date for the Type II and Type IV, their October monthly maximums did occur on the 14th. June 29th appears to be the exception with a lower than average temperature change and higher wind speeds. May 18th was the warmest day in May and October 14th was the warmest day in October. There were several days with recorded highs above 90°F (32°C) in June. Despite this, none of the maximum recorded vertical gradients occurred on particularly hot days considering typical summer temperatures in the southern United States. In Norman, OK, temperatures frequently approached 100°F (38°C) but maximum gradients were never recorded on these days. In the months of June, July, August, and September, temperatures climbed above 90°F (32°C) 48 times in Norman, OK, with 20 of those days eclipsing 95°F (35°C). While this study was initiated with the intent of investigating if design procedures needed to be adjusted for extreme heat waves, the most extreme thermal gradients never occurred during an extreme heat event. This data would suggest that, concerning temperature gradients, extreme heat is not the critical design condition.

4.1.2. Transverse Gradients

Transverse temperature gradients are those between the vertical faces of the bridge girders. Transverse gradients were observed in the top and bottom flanges of each beam segment. All test specimens were oriented in the east-west direction so that the southern faces were exposed to sunlight and the northern faces were shaded throughout the day. As with the vertical gradients, the Type II and Type IV beams experienced similar transverse gradients. Figure 4.5 displays the maximum transverse gradients in both the top and bottom flanges for the Type II section. Only summer and fall months are displayed as this is when the worst transverse gradients were recorded. For better visual comparison, the transverse gradients have already been adjusted to the minimum temperature at zero, showing just temperature difference, not actual recorded temperature. The readings collected from the surface thermocouples have not been included in the analysis of the transverse gradients for the reasons stated in Section 4.1.1.

The maximum transverse gradient measured in each flange is denoted by a solid black line. In the top flange, the May and July gradients from the Arkansas test site both appear to be outliers to the typical gradient experienced. However, the July reading is the maximum measured gradient. During thermal response analysis, both the June and July gradients were investigated. These gradients were recorded on June 10th at 4:00pm and July 27th at 1:00pm. For the bottom flange, the gradients were more consistent in their shape. The maximum transverse gradient in the bottom flange of a Type II occurred on August 25th at 3:40pm. Both maximums occurred at the Arkansas location.

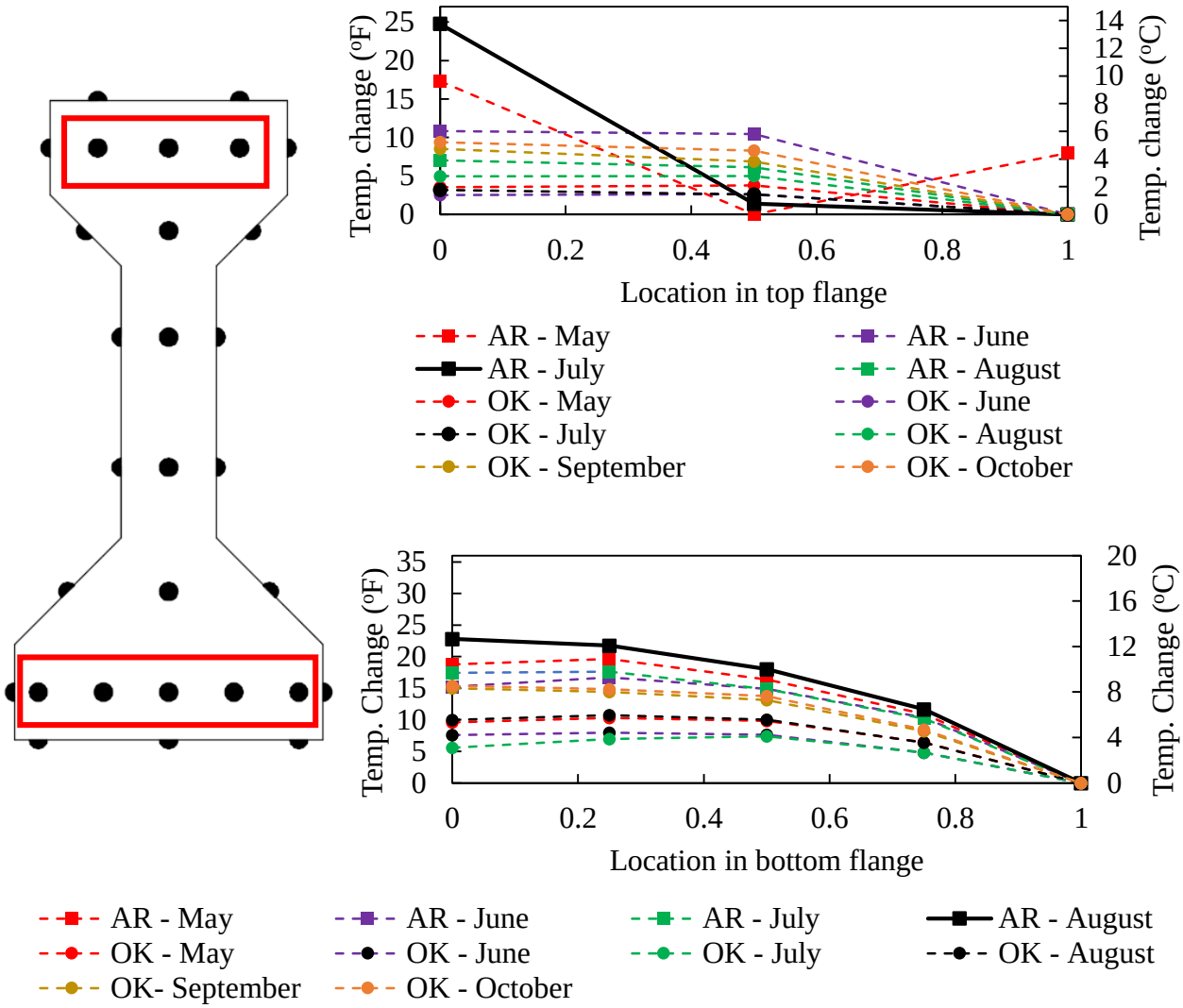

Figure 4.5 - Type II measured transverse temperature gradients in top and bottom flange

The measured transverse gradients for the Type IV section are displayed in Figure 4.6. It should be noted that there was a malfunction with a thermocouple in the top flange of the Type IV section at the Fayetteville location and only the complete gradients are reported in Figure 4.6. The maximum gradients in each flange are denoted by the solid black line. The maximum transverse gradient in the top flange of a Type IV was recorded at the Oklahoma test site on October 14th at 1:30pm. The maximum transverse gradient in the bottom flange of a Type IV was recorded at the Arkansas test site on October 13th at 3:25pm.

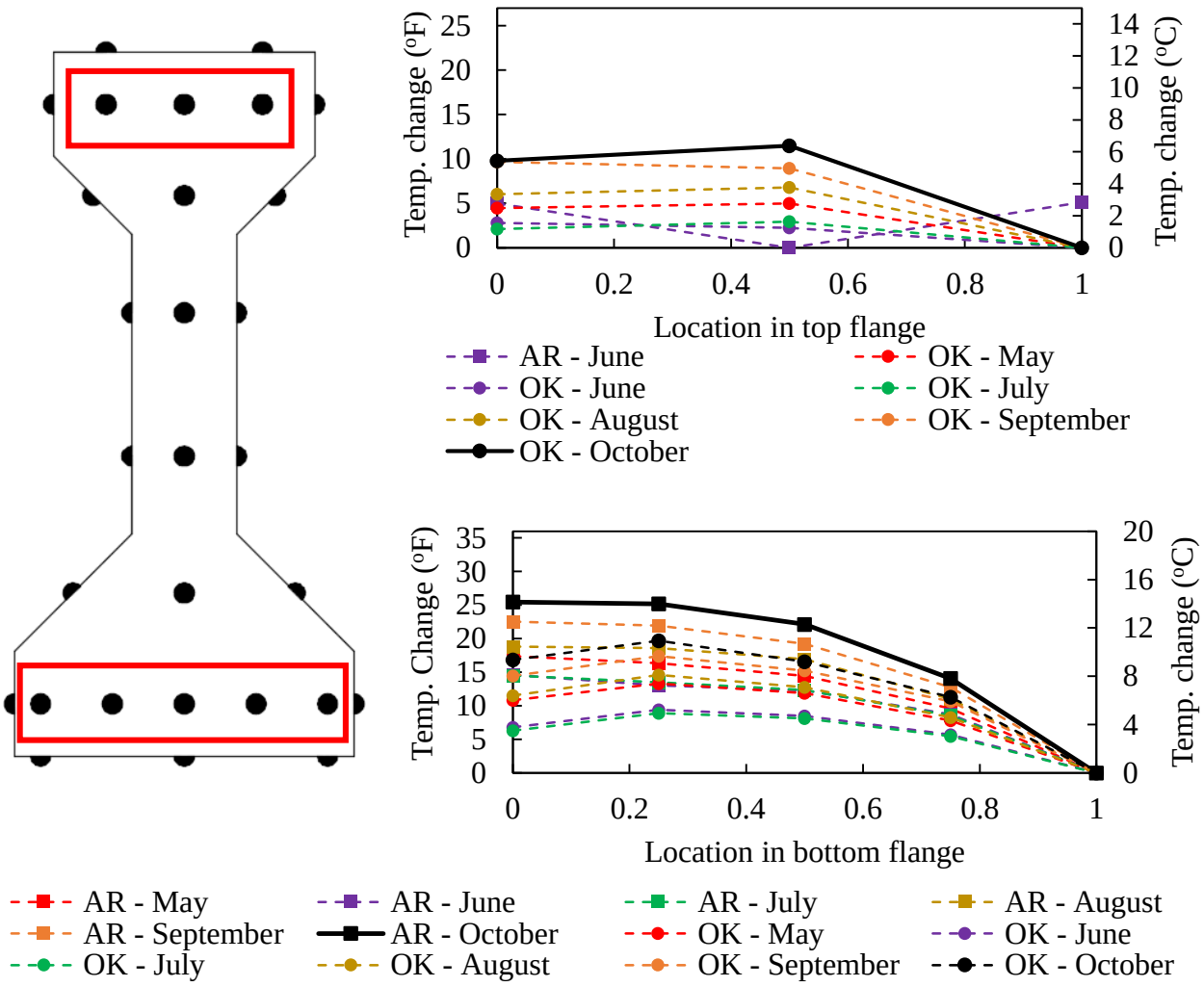

Figure 4.6 - Type IV measured transverse temperature gradients in top and bottom flange

The measured transverse gradients for the Type V section are displayed in Figure 4.7. Gradients are only recorded for September, October, November, and December of 2015. There was only a Type V test segment at the Arkansas site. The maximum transverse gradient in the top flange was recorded on September 22nd at 12:00pm. The maximum transverse gradient in the bottom flange of the Type V was recorded on November 12th at 2:40pm.

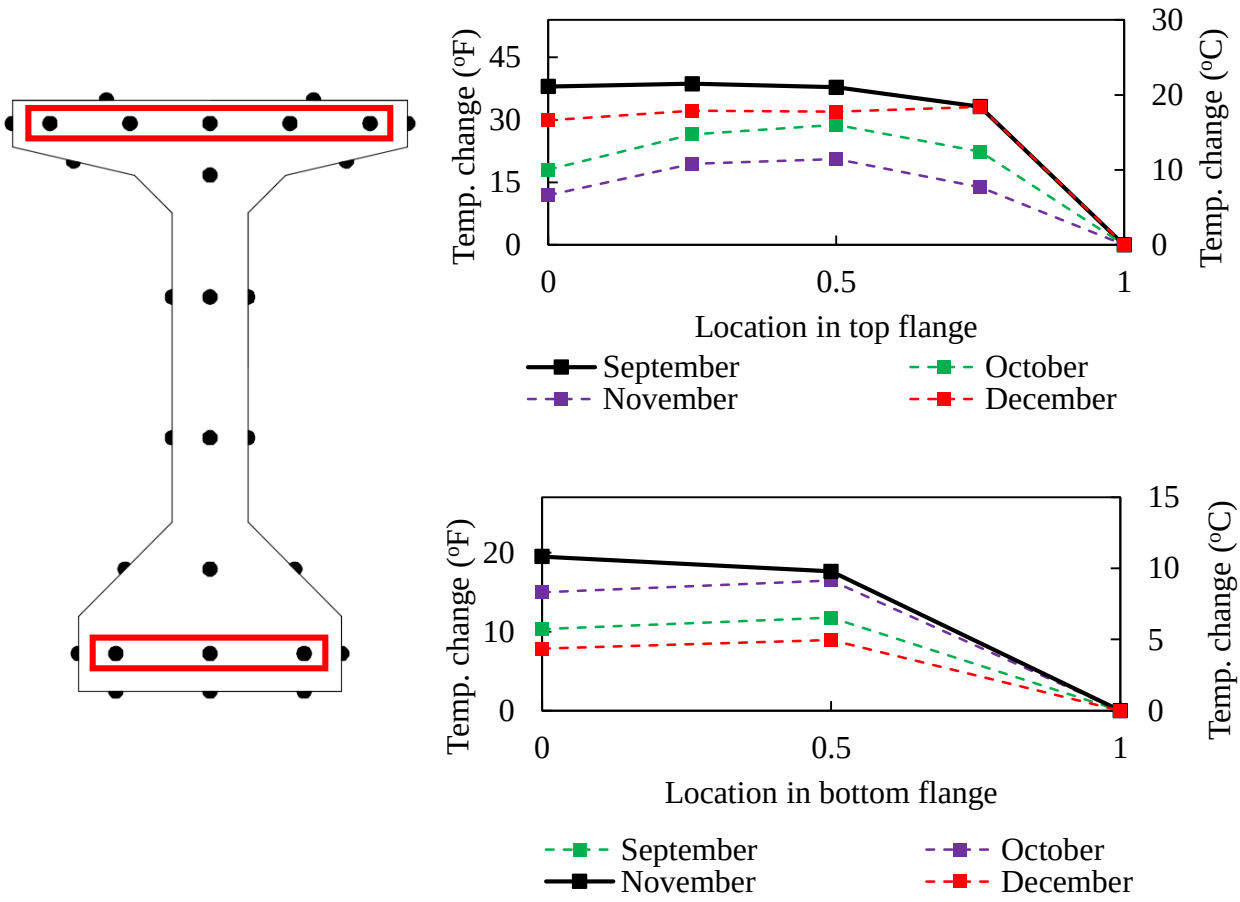

Figure 4.7 - Type V measured transverse temperature gradients in top and bottom flange

While not as consistent as the vertical gradients, the measured transverse gradients also occurred mostly in the mid-afternoon near peak solar radiation. All of the observed transverse gradients follow the expected pattern given girder orientation - temperatures were the highest on the southern sides of the beams and decreased towards the northern side.

The environmental conditions on the days of maximum transverse thermal gradients are listed in Table 4.3. The June and July dates listed in this table were both the hottest days of the month. As with vertical gradients, the maximum transverse thermal gradients were observed on days with large daily temperature variations and no precipitation. Of the dates listed, only July 27 had a below average temperature range for the month. It appears that low wind speeds also result in larger temperature gradients in most cases. The October and November dates had higher

wind speeds than the other dates considered in Table 4.3, however those dates had temperature ranges well above the monthly averages.

Table 4.3 – Environmental conditions on days of maximum observed transverse gradients

Site	Date	Max. Temp.	Min. Temp.	Temp. Change	Max. Temp.	Min. Temp.	Temp. Change	Precip.	Avg. Wind	Avg. Wind
		[ºF]	[ºF]	[ºF]	[ºC]	[ºC]	[ºC]	[in.]	[m/s]	[mph]
AR	10-Jun	90.0	61.0	29.0	32.2	16.1	16.1	0	1.8	4.0
AR	27-Jul	91.9	75.0	16.9	33.3	23.9	9.4	0	1.7	3.8
AR	25-Aug	82.9	48.9	34.0	28.3	9.4	18.9	0	0.5	1.1
AR	22-Sep	84.0	57.0	27.0	28.9	13.9	15.0	0	0.9	2.0
AR	13-Oct	93.0	55.0	38.0	33.9	12.8	21.1	0	3.7	8.3
OK	14-Oct	79.0	39.0	40.0	26.1	3.9	22.2	0	1.9	4.3
AR	12-Nov	60.1	32.0	28.1	15.6	0.0	15.6	0	3.4	7.6

4.2. Strain Measurements

As a measure of the accuracy of the recorded temperatures, strain readings were manually taken using a DEMEC gauge. DEMEC points were attached to the south facing surfaces of the Type IV and Type V beam segments at the Arkansas test site. On October 15, 2015, a strain measurement experiment was conducted on the Type V. Readings were first taken before sunrise and those measurements were used as the zero expansion point. Strain was then measured at four different times throughout the day. From these measurements, a change in length over the course of the day was established. This change of length was found to be the greatest at 3:45pm. Assuming any measured expansion was the sole result of a rise in temperature, a typical coefficient of thermal expansion (11.7×10^{-6} /ºC or 6.50×10^{-6} /ºF) was used to calculate a theoretical temperature. This theoretical temperature rise is compared with the measured temperature rise over the same time period in Figure 4.8.

The same process was followed on November 2nd, 2015 for the Type IV girder segment at the Arkansas test site. The maximum expansion was measured at 3:30pm on this date. Figure 4.9

displays a comparison of the theoretical temperature rise based on strain readings versus the measured temperature rise over that same period for the Type IV girder. Figures 4.8 and 4.9 also have photographs with the approximate locations of the DEMEC measurement points highlighted.

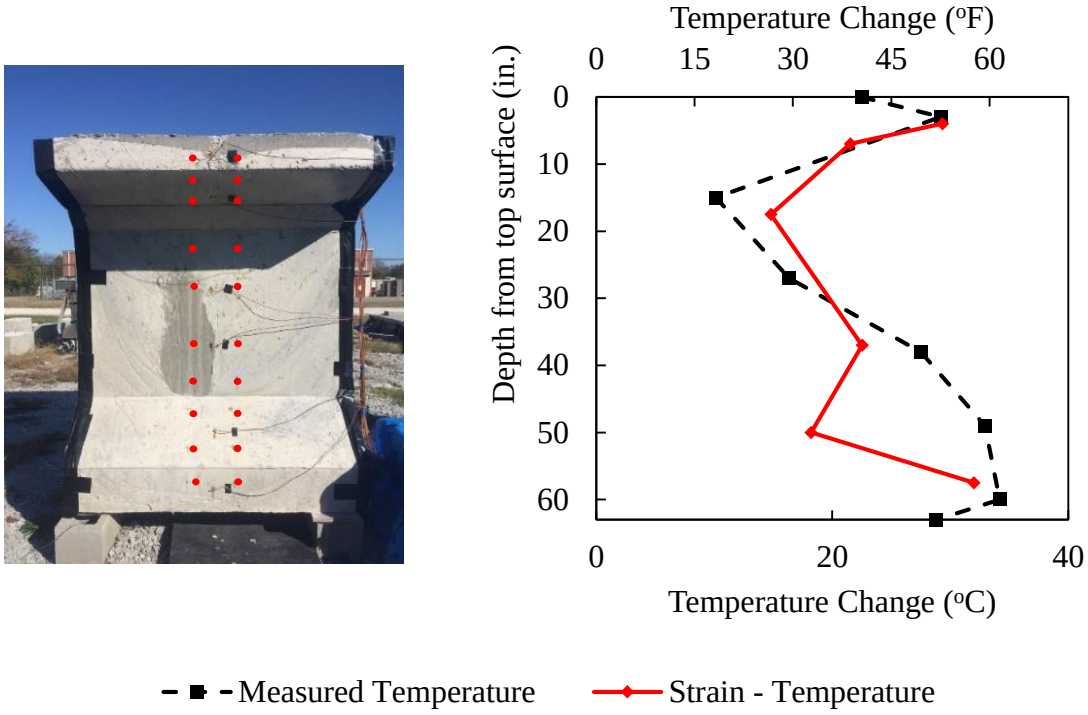

Figure 4.8 - Comparison of theoretical temperature rise from strain readings vs. measured temperature rise in Type V on October 15 at 3:45pm – Arkansas test site

Both comparisons show good agreement using this coefficient of thermal expansion. The measurements match well in the upper portions of the girder and deviate slightly in the lower portions. The locations of greatest temperature rise in both the Type V and Type IV are consistent between the two methods. This is not meant to be a perfect comparison as there some errors between the two methods, the main one being that expansion readings were taken on the outside face of the beam and compared with the internal thermocouples down the middle of the

beam section. However, this experiment does allow the conclusion that thermocouple temperature readings can be accurately estimated with physical measurements.

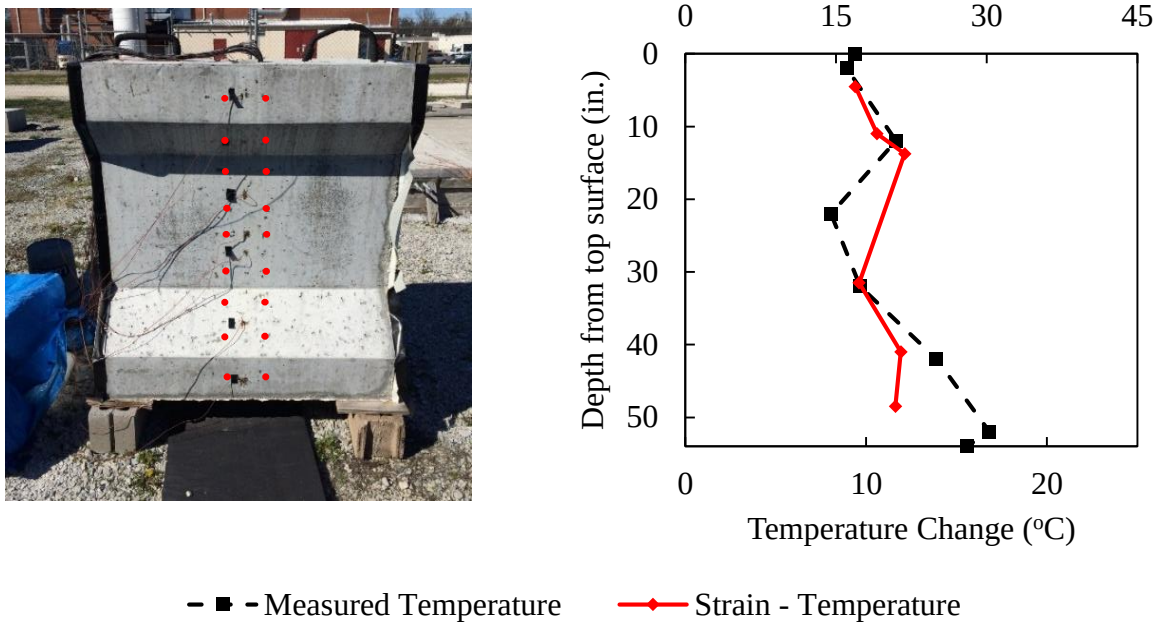

Figure 4.9 - Comparison of theoretical temperature rise from strain readings vs. measured temperature rise in Type IV on November 2 at 3:30pm – Arkansas test site

4.3. Comparison to past results

Figures 4.10, 4.11, and 4.12 compare the maximum measured vertical temperature gradients to the AASHTO design gradient and the gradient recommended by Lee (2010). The AASHTO gradient applies to solar radiation Zone 2.The Brownsville, TX location was used to determine the Lee (2010) gradient. These locations most closely to apply to the Arkansas-Oklahoma area of the United States.

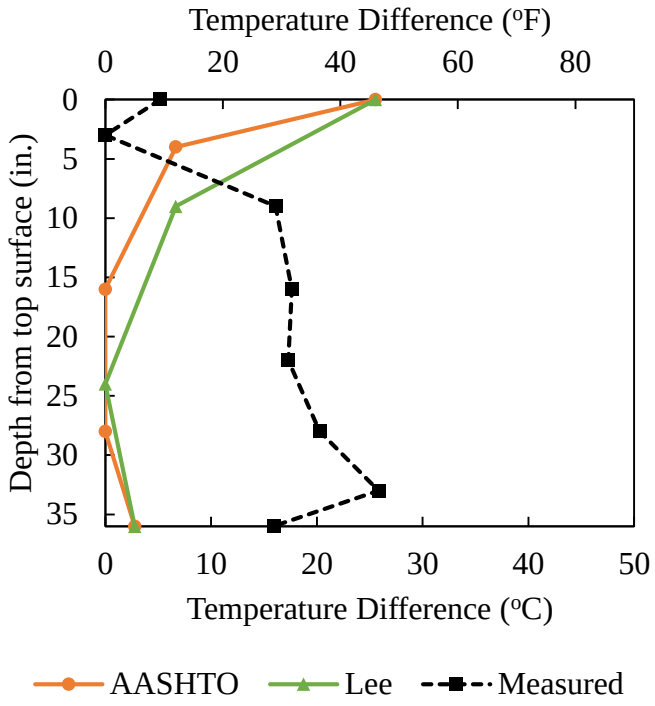

Figure 4.10 - Type II comparison of vertical thermal gradients

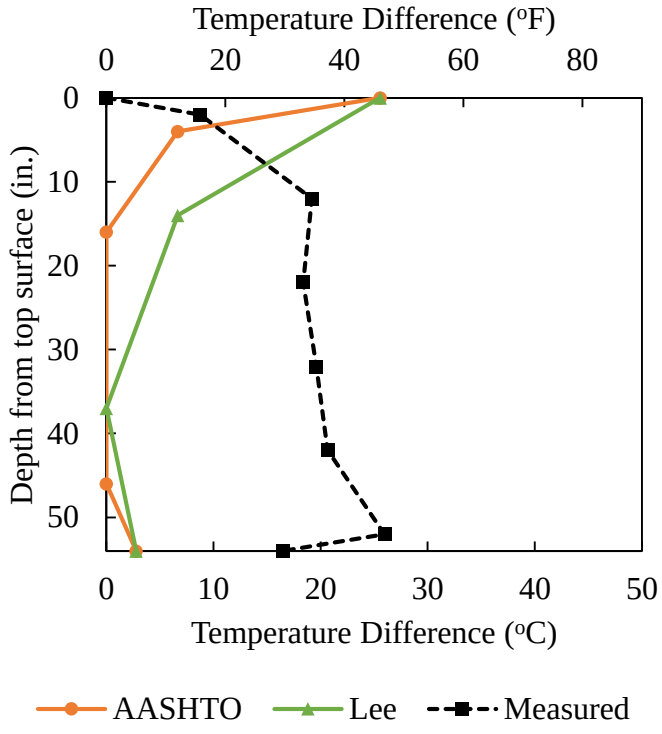

Figure 4.11 - Type IV comparison of vertical thermal gradients

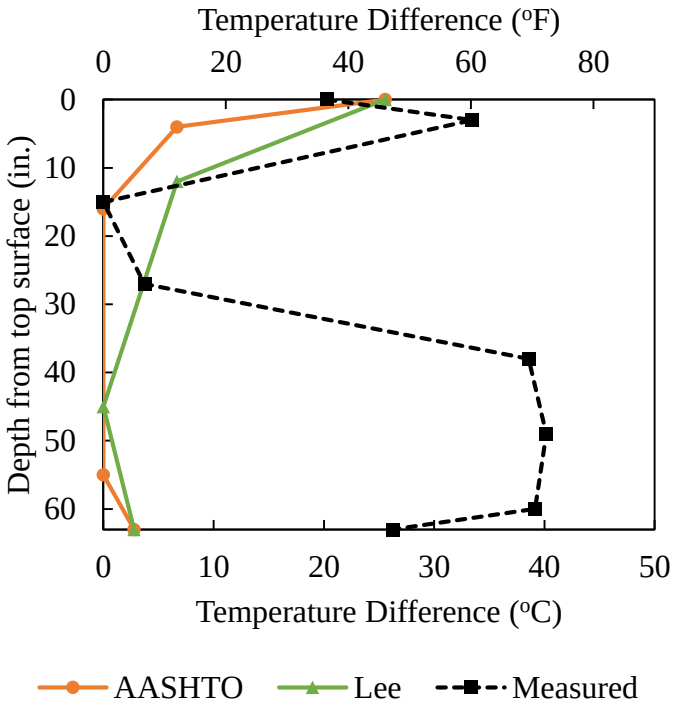

Figure 4.12 - Type V comparison of vertical thermal gradients

These figures display once again the differences between the design standards and what was measured during this experiment. The measured temperature increase in the bottom flange of the Type V could be attributed to the fact that the maximum gradient was observed during the fall months, meaning a shallower solar angle and more direct sunlight on the vertical faces of the beam. This same explanation cannot be applied to the measured temperatures in the Type II and Type IV however. The AASHTO LRFD Bridge Design specifications do include a comment in the temperature gradient section (AASHTO Section 3.12.3) that provides the guidelines for a negative temperature gradient. For a plain concrete deck, positive design values are to be multiplied by -0.30. While this is meant for wintertime conditions when the concrete maintains higher temperatures than the ambient air, it could offer a useful comparison with the

temperatures observed specifically in the Type II and Type IV sections. The measured gradients compared against the AASHTO negative gradient are displayed in Figure 4.13.

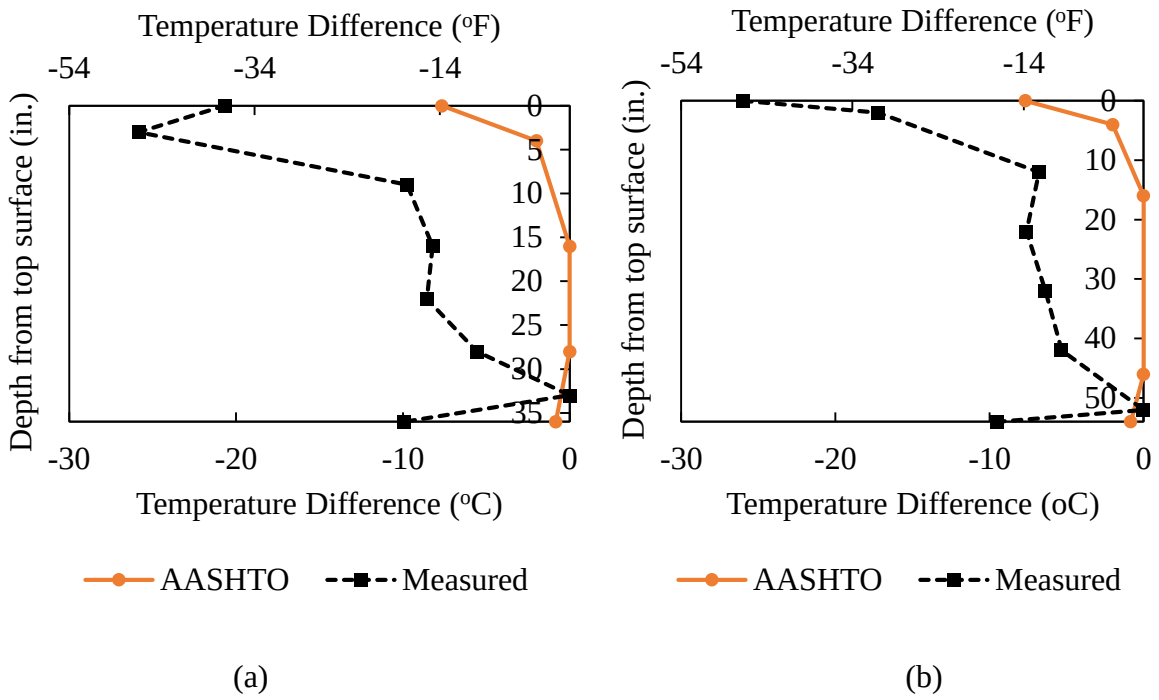

Figure 4.13 - Negative AASHTO vertical temperature gradient vs. measured vertical gradient (adjusted as negative gradient) for (a) Type II and (b) Type IV

The magnitude of temperature change is much higher in the measured gradients but the overall shape could still be described as a negative gradient based on these results. The top flange having consistently the lowest recorded temperatures in the Type II and Type IV sections was an unexpected outcome. Section 4.5 investigates how the response of concrete bridge girders is affected by different gradients such as the ones measured in this research.

The AASHTO design specifications do not include a transverse design gradient to be used for concrete bridge girders, but Lee's 2010 study on a BT-63 concrete beam does. Figures 4.14 and 4.15 display the measured transverse gradients for the Type II and IV sections

compared to Lee's recommended transverse gradients. Figures 4.16 and 4.17 displays the same comparison for the top and bottom flanges of the Type V.

In the top flanges of all sections, the overall magnitude of temperature change is similar, but the shapes are not. They II/IV display a better match than the Type V. In the bottom flanges of all sections, Lee's findings recommend a higher gradient than that the ones measured in this study.

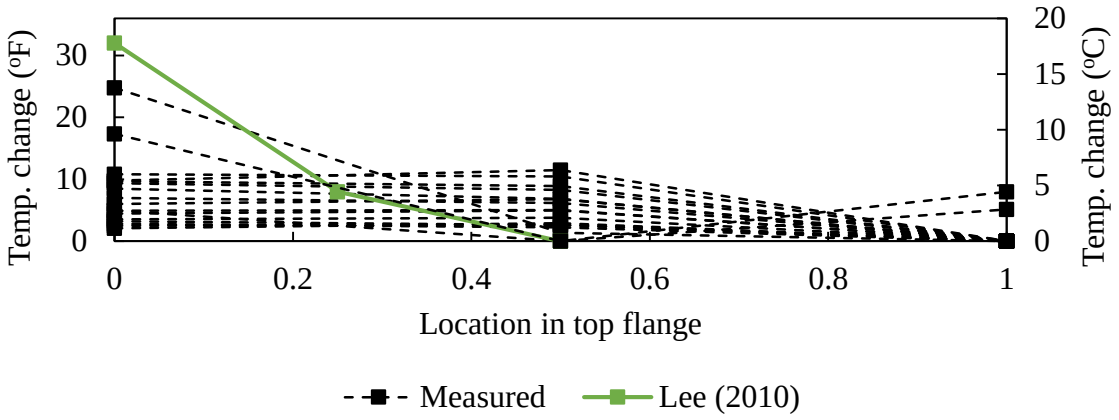

Figure 4.14 – Type II/IV top flange comparison of transverse thermal gradients

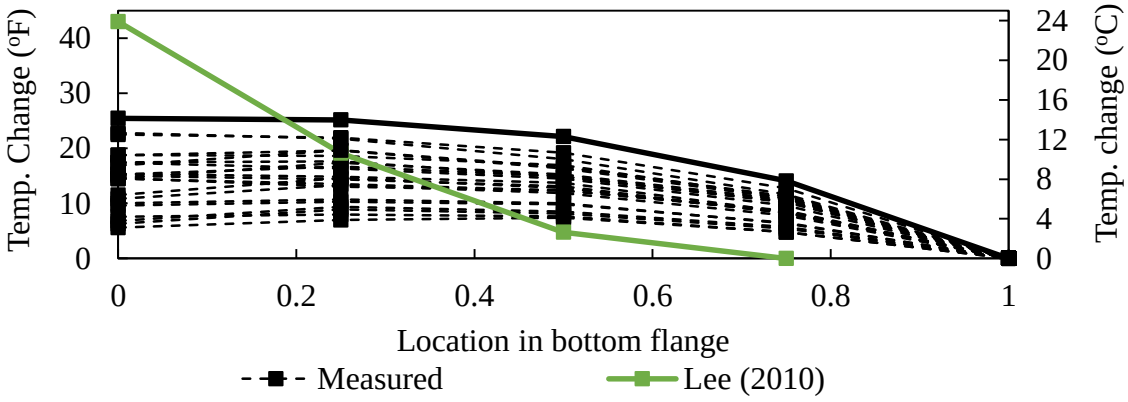

Figure 4.15 – Type II/IV bottom flange comparison of transverse thermal gradients

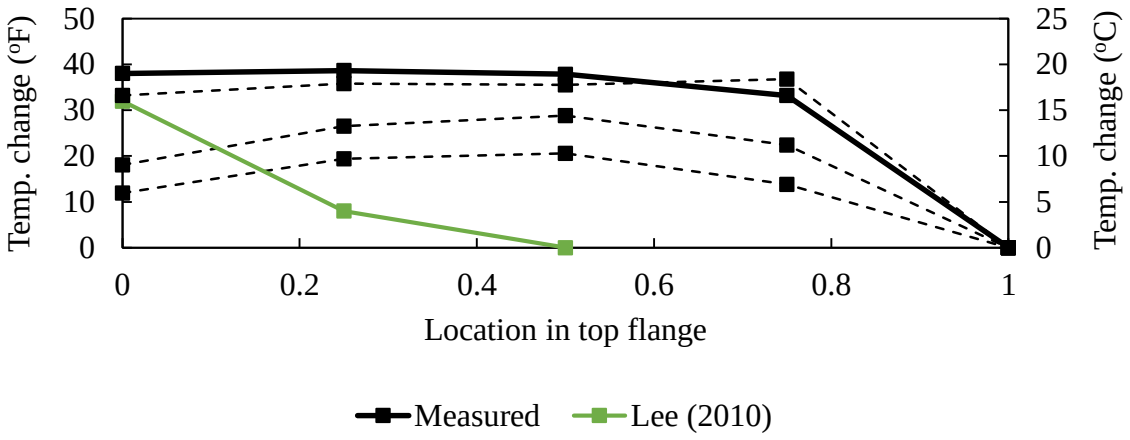

Figure 4.16 – Type V top flange comparison of transverse thermal gradients

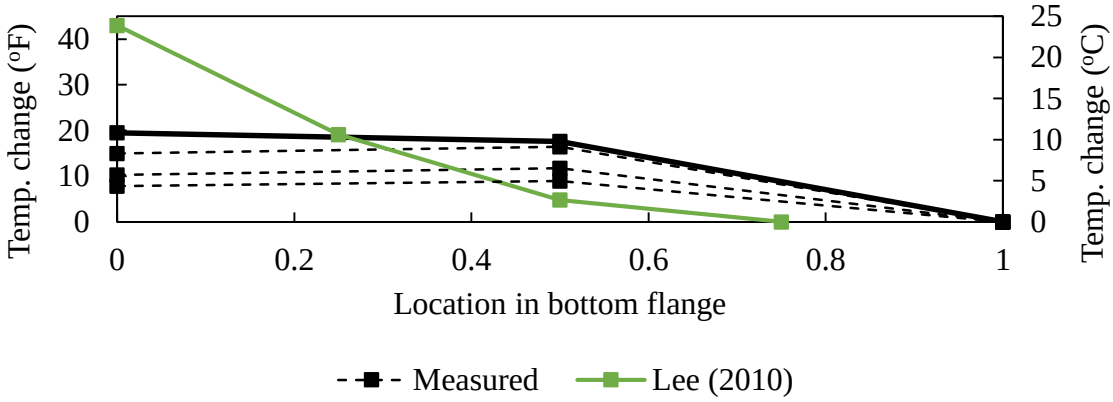

Figure 4.17 – Type V bottom flange comparison of transverse thermal gradients

4.4. Temperature Modeling

The next phase of this project was to reproduce the measured temperature gradients using a heat transfer model. To build such a model, the solar radiation input was first calculated. This was accomplished using the method outlined in Section 3.4. Figure 4.18 displays a comparison between the predicted solar radiation in Fayetteville, AR on October 28, 2015 versus the reported NOAA values from the closest measurement site. From this comparison, it can be concluded that with the proper inputs (location, day of year, and average total daily radiation from Table 3.1) the incident solar radiation on a horizontal surface can be accurately predicted.

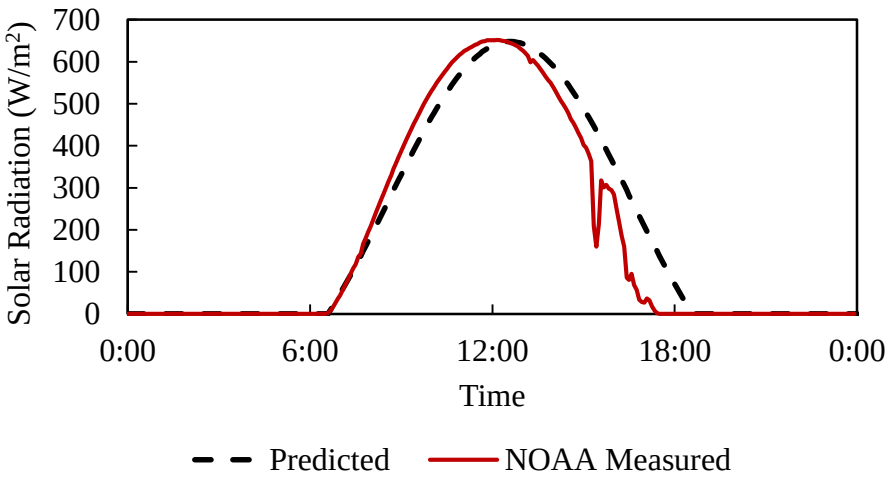

Figure 4.18 - Predicted vs. measured solar radiation in Fayetteville, AR - October 28, 2015

Using HACON modeling software, two-dimensional cross sections were constructed and the appropriate adjusted solar radiation was applied to each surface. The solar radiation input was adjusted for incline of the surface when necessary. Models were built to run over the course of three days at a minimum. This allowed the sections to go through several heating and cooling cycles and accounted for any heat retained in the concrete during nighttime hours. For each section, the environmental conditions on the day when the maximum gradients were measured were used as inputs. This means, for comparing the vertical gradients, the Type II model was run from May 16th-18th, the Type IV was run from June 27th-29th, and the Type V was run from October 12th-14th. The material properties used for these models are listed in Table 4.4.

Table 4.4: Summary of material properties

Property	SI Units		US Units	
Thermal Conductivity	2.0	[W/^{o}C]	0.35	[BTU/hr-ft-^{o}F]
Specific Heat	900	[J/kg-^{o}C]	0.21	[BTU/lb-^{o}F]
Coefficient of Thermal Expansion	6.50E-06	[/ ^{o}C]	1.17E-05	[/ ^{o}F]
Compressive Strength	55.2	[MPa]	8.0	[ksi]
Modulus of Elasticity	35150	[MPa]	5098	[ksi]
Mass Density	2403	[kg/m^3]	150	[lb/ft^3]

Figures 4.19, 4.20, and 4.21 display the modeled temperature gradients and the measured temperature gradients for the Type II, Type IV, and Type V respectively.

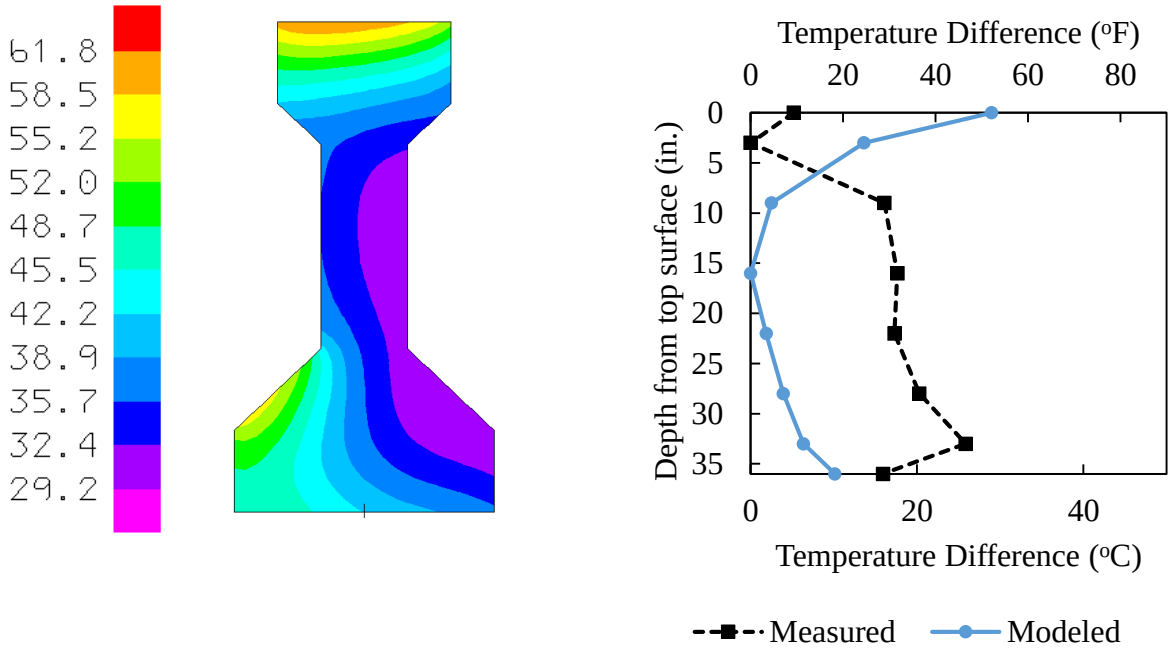

Figure 4.19 - Type II maximum vertical temperature gradients (measured and modeled) at 3:00pm on May 18, 2015 in Fayetteville, AR

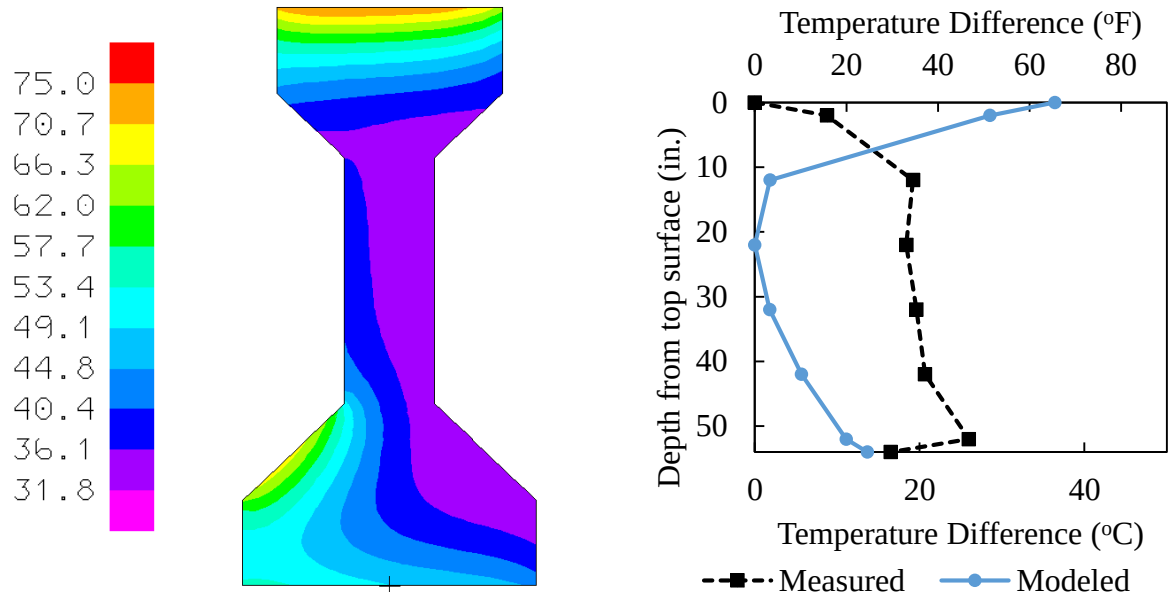

Figure 4.20 - Type IV maximum vertical temperature gradients (measured and modeled) at 2:00pm on June 29, 2015 in Fayetteville, AR

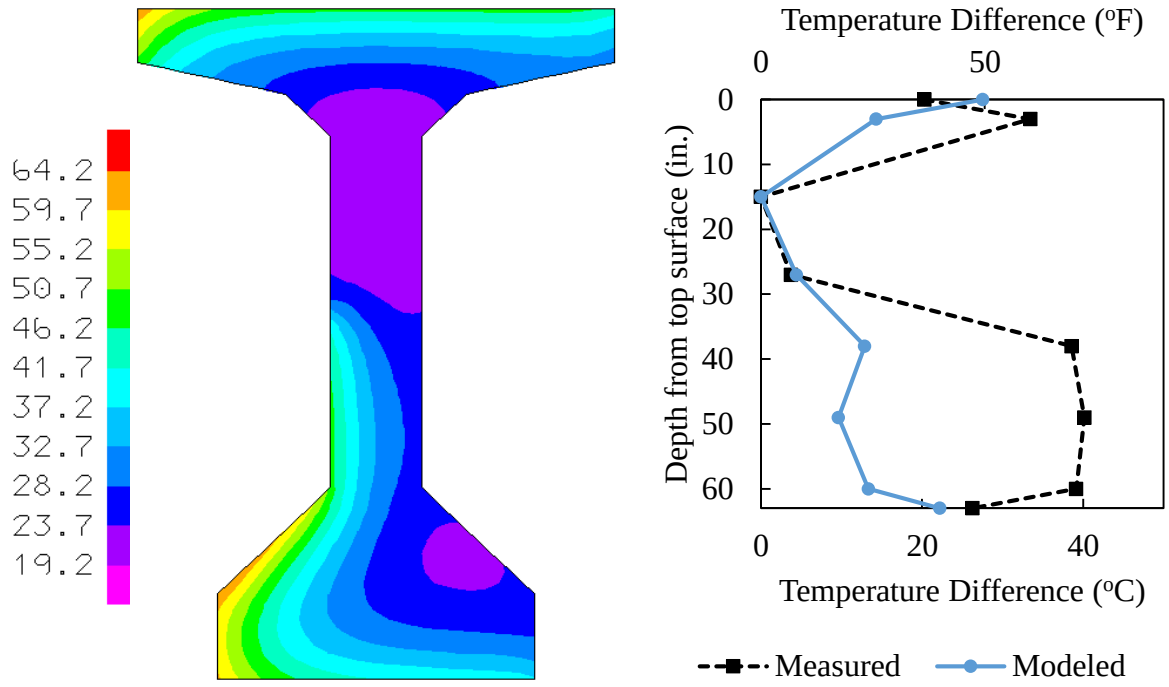

Figure 4.21 - Type V maximum vertical temperature gradients (measured and modeled) at 12:45pm on October 14, 2015 in Fayetteville, AR

These three figures indicate that there is not a strong match between the modeled and the measured vertical thermal gradients. In the Type II and Type IV sections, the lower portion of the beams follow a similar pattern (although different magnitudes) but the top flanges show different results. In the Type V section, the top flange shows good agreement while the bottom portion is much warmer in the measured gradient than in the modeled. It is unclear as to why these differences occur. Altering the material properties affected the gradients very little, as was determined by previous researchers and discussed in Section 2.1 (Lee, 2010). While the amount of solar radiation incurred by each surface could be varied, this would not follow the established practices for determining these values and would thus be manipulating inputs to achieve desired outputs. This modeling process that must be revisited in further research to address these discrepancies.

Transverse gradients were also observed the heat transfer model. Simulations over several different dates when maximum transverse gradients were measured were used as the inputs for these models. Only the maximums are recorded in the following figures. Figures 4.22, and 4.23 display the maximum transverse gradients from the modeling process for the Type II and IV beams against the maximum measured gradients. Because of the similarities, the Type II and Type IV gradients were grouped together for this analysis. The monthly maximums are left on both graphs to illustrate how the modeled gradients compare. Figures 4.24 and 4.25 display the same comparison for the Type V beam section.

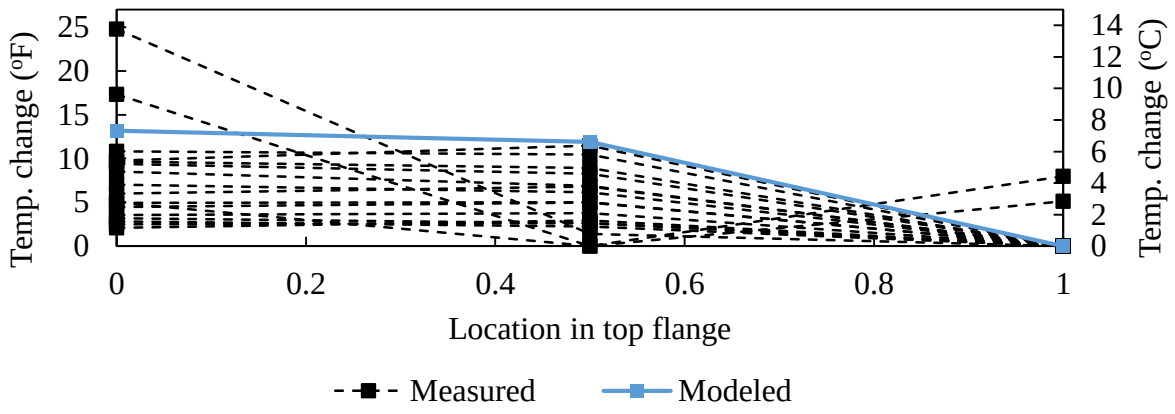

Figure 4.22 - Type II/IV maximum transverse thermal gradients (measured and modeled) in top flange

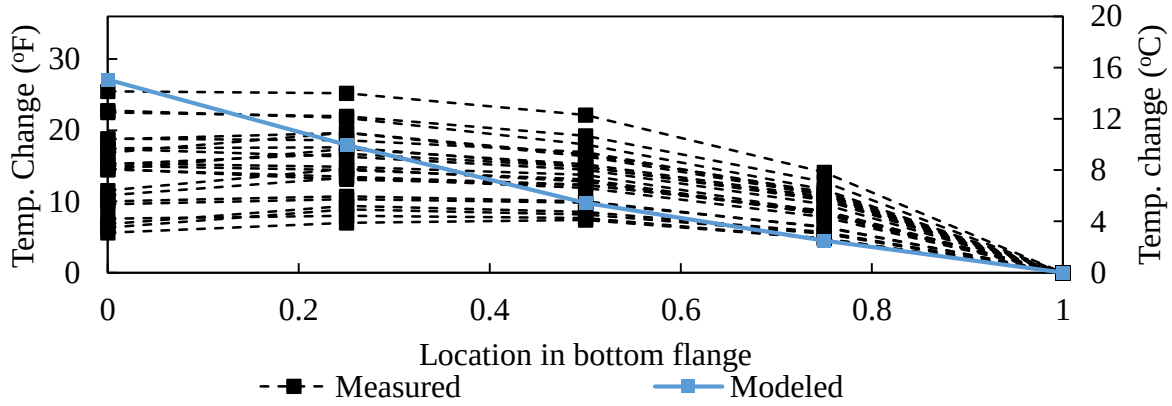

Figure 4.23 - Type II/IV maximum transverse thermal gradients (measured and modeled) in bottom flange

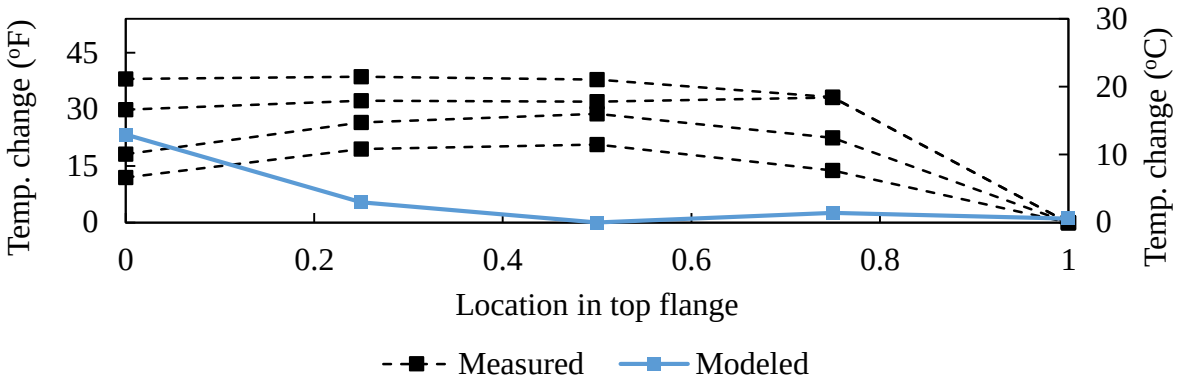

Figure 4.24 - Type V maximum transverse thermal gradients (measured and modeled) in top flange

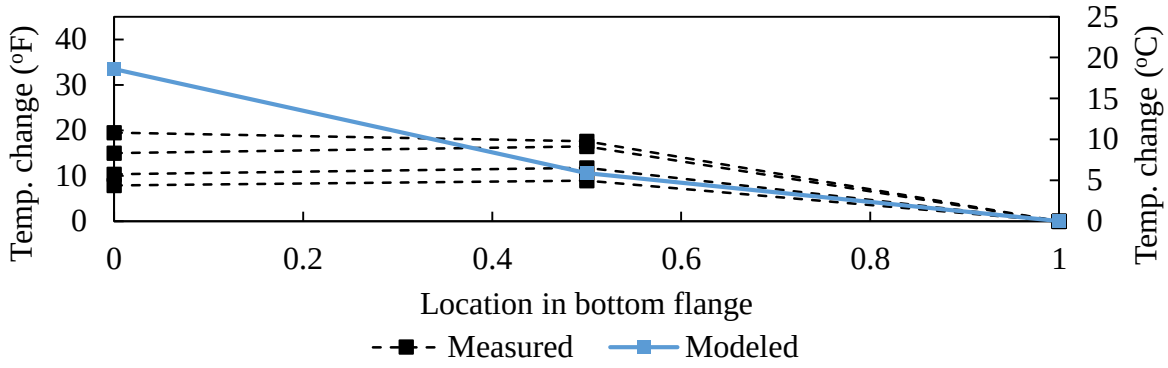

Figure 4.25 - Type V maximum transverse thermal gradients (measured and modeled) in bottom flange

The modeled transverse gradients show better agreement with measured values than those of the vertical gradients. Only the top flange of the Top V fails to follow the trend of measured values. The shape in bottom flange of the Type II/IV is different, but the overall effects of such a gradient will be similar to those of the measured gradients.

4.5. Thermal response of full scale girders

The response of prestressed concrete bridge girders to vertical and transverse temperature gradients was studied using three-dimensional solid element models built in SAP2000. The material properties necessary for this analysis are summarized in Table 4.4, which can be found in Section 4.4.

First, the two-dimensional internal stresses that would be developed from non-linear vertical temperature gradients were calculated using the process outlined in Section 3.5. This method calculates only the stress that would result from non-linear temperature profiles as a simply supported beam. It neglects any stress from self-weight or superimposed loads. The resultant stress profiles for the three gradients that were investigated (AASHTO, Lee (2010), and measured) are shown for a Type II, Type IV, and Type V in Figures 4.26, 4.27, and 4.28 respectively. For these figures, tension is displayed as positive stress values and compression as negative. This same sign convention was used for all further analysis.

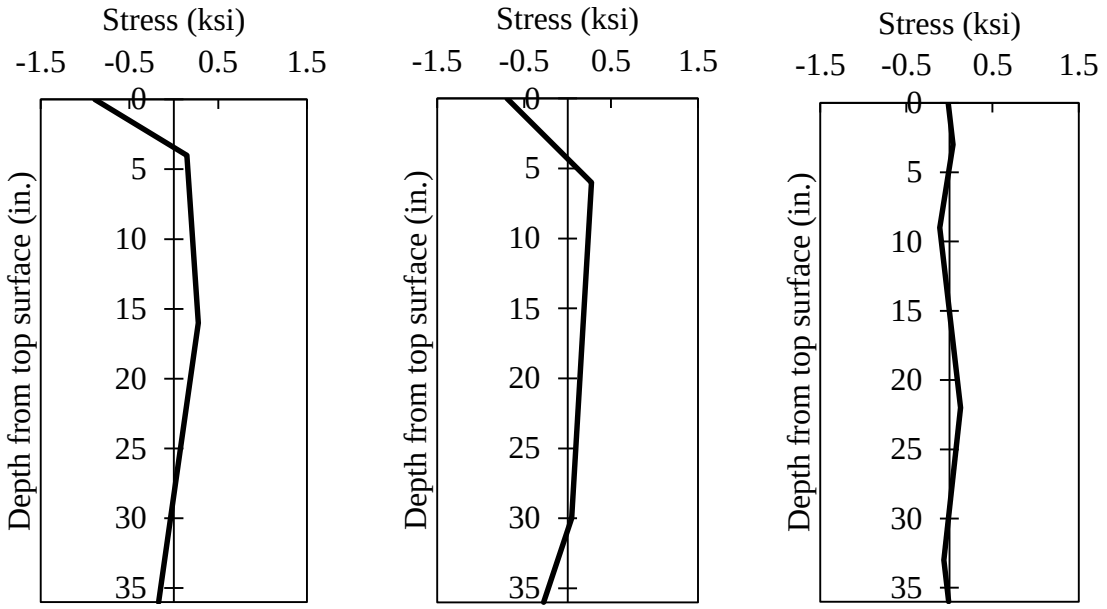

Figure 4.26 - Type II internal stress profile resulting from (a) AASHTO (b) Lee (2010) and (c) measured temperatures

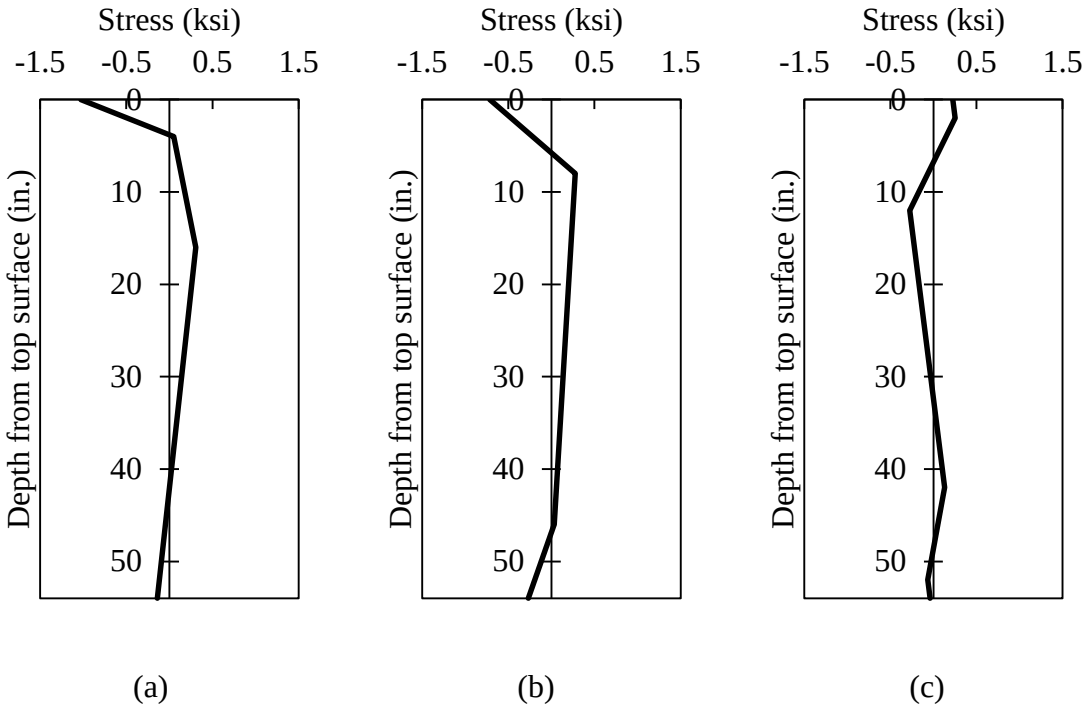

Figure 4.27 - Type IV internal stress profile resulting from (a) AASHTO (b) Lee (2010) and (c) measured temperatures

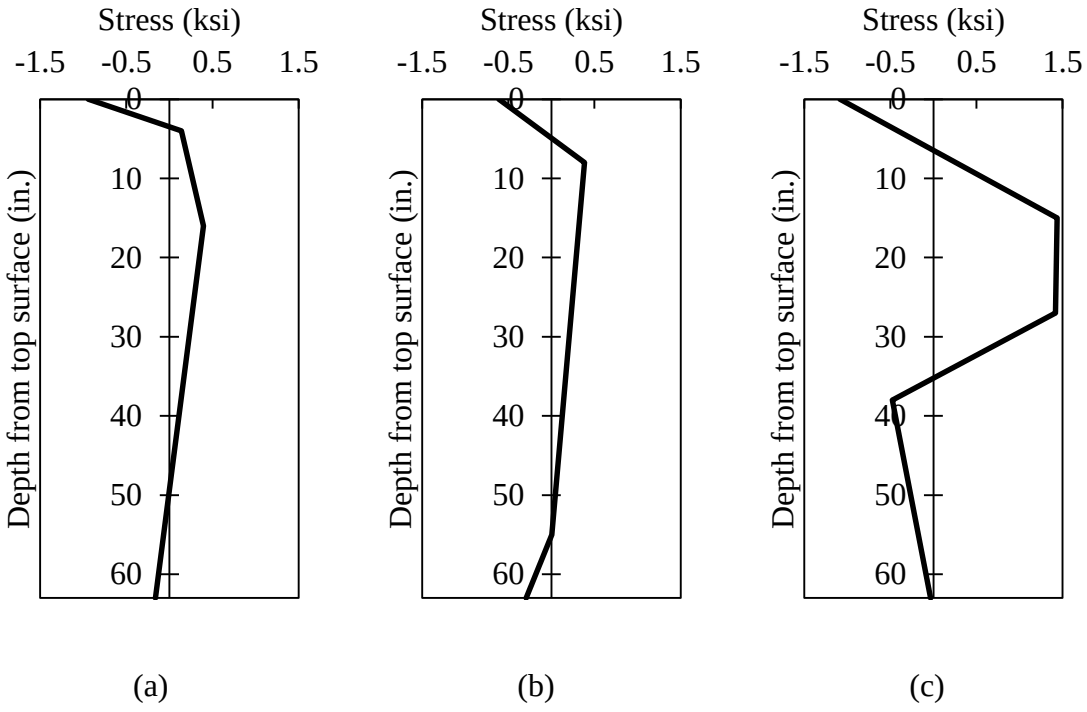

Figure 4.28 - Type V internal stress profile resulting from (a) AASHTO (b) Lee (2010) and (c) measured temperatures

Simple span girders were then constructed in SAP2000 to confirm these profiles. By using the same material properties listed in Table 4.3 (except neglecting self-weight) the stress profiles in Figures 4.26, 4.27, and 4.28 were confirmed exactly in SAP2000. These stresses are consistent regardless of span length and take place at mid-span of a simply supported beam. This confirmation allowed more detailed and realistic models to be constructed in SAP2000. Typical span lengths were chosen for each girder: 60 feet for the Type II, 100 feet for the type IV, and 125 feet for the Type V. Next, simple pin and roller supports were replaced with translational and rotational springs to model elastomeric bearing pads used in typical simple span bridge construction. While the stiffness of bearing pads is dependent on several geometric parameters of the pad, the bearing pads used for the three girders being investigated would be similar and thus average values were used for all three. A horizontal stiffness of 10 kip/in, a vertical stiffness of 6530 kip/in, and a rotational stiffness of 3650 kip-in/in was used in all models.

To further understand the global response of bridge girders to temperature gradients, a prestressing force was also applied. The total force of the prestressing strand group after long term losses was applied at the center of gravity of the strand group on each end of the girder. This created elevated stresses at the girder ends, but since the focus of this modeling experiment was to determine stresses and deflections at mid-span, this is an adequate method. The long term losses were determined using the detailed AASHTO method. 0.6 inch strands (A=0.217 in^2) were used for all sections. The prestressing forces are summarized in Table 4.5.

Table 4.5 – Summary of prestressing forces

Section	No. of Strands	Jacking Force	Long Term Losses	Final PS Force	Ecc. from bottom
-	-	[ksi]	[ksi]	[kip]	[in.]
Type II	26	202.5	75	719	4.46
Type IV	60	202.5	75	1660	6.27
Type V	72	202.5	70	2070	7.06

In addition to these factors, transverse thermal gradients and vertical thermal gradients were applied concurrently in the models. This allowed for a full analysis of the stresses that would result from the combined gradients. Maximum stress and displacements were recorded at mid-span under various loading conditions: self-weight only, self-weight and prestressing force, thermal loads with no self-weight, thermal loads with self-weight, and finally all loads combined. The results of this investigation are summarized in Table 4.6 and 4.7.

Table 4.6 – Mid-span stresses of prestressed concrete bridge girders under measured temperature gradients

Measured Temperature		Top Stress	Bottom Stress	Max Comp.	Location	Max Tension	Location
		[ksi]	[ksi]	[ksi]	-	[ksi]	-
Type II	Self-Weight (SW)	0.82 (C)	0.64 (T)	0.82	Bottom Fiber	0.64	Top Fiber
	PS + Self Weight	**0.42 (T)**	**3.8 (C)**	**3.8**	**Bottom Fiber**	**0.42**	**Top Fiber**
	Temperature	0.33 (T)	0.30 (T)	0.25	Bottom Flange	0.33	Top Fiber
	Temp. + SW	0.66 (C)	0.95 (T)	0.75	Top Flange	0.95	Bottom Fiber
	Combined	**0.67 (T)**	**3.8 (C)**	**2.39**	**Bottom Fiber**	**0.67**	**Top Fiber**
Type IV	Self-Weight (SW)	1.37 (C.)	1.15 (T)	1.37	Bottom Fiber	1.15	Top Fiber
	PS + Self Weight	**0.11 (C)**	**3.7 (C)**	**3.7**	**Bottom Fiber**	-	-
	Temperature	0.19 (T)	0.18 (C)	0.25	Bottom Flange	0.27	Web
	Temp. + SW	1.34 (C)	1.39 (T)	1.34	Bottom Fiber	1.39	Top Fiber
	Combined	**0.06 (T)**	**3.9 (C)**	**3.9**	**Bottom Fiber**	**0.06**	**Top Edge**
Type V	Self-Weight (SW)	1.47 (C)	1.49 (T)	1.47	Top Fiber	1.49	Bottom Fiber
	PS + Self Weight	**0.50 (C)**	**3.6 (C)**	**3.6**	**Bottom Fiber**	-	-
	Temperature	1.42 (C)	0.37 (C)	1.42	Top Fiber	2.05	Top of Web
	Temp. + SW	2.88 (C)	1.39 (T)	2.88	Top Fiber	1.75	Mid Web
	Combined	**1.91 (C)**	**3.93 (C)**	**3.93**	**Bottom Fiber**	**0.82**	**Top of Web**

Several observations can be made from these results. First, observing the beam with prestressing force and with prestressing force combined with temperature gradient loading, the tensile forces in the beam increased in all cases but in different locations. The maximum compressive force decreased in the Type II while increasing the Type IV and Type V. In all cases, the upward deflection, or camber, of the beam was decreased. The Type V experienced the

greatest impacts from application of the thermal gradients. The transverse temperature gradients caused varying amounts of lateral deflection in the different girder types. All three lateral displacements can be considered relatively small however, the deflections correspond to values of approximately L/1500 for the Type II and Type IV girders, and L/1000 for the Type V girder.

Table 4.7 – Mid-span deflections of prestressed concrete bridge girders under measured temperature gradients

Measured Temperature		Max Lateral Displacement [in]	Max Vertical Displacement [in]
Type II	Self-Weight	-	-0.43
	PS + Self Weight	**-**	**1.6**
	Temperature	0.47	-0.63
	Temp. + Self Weight	0.47	-1.1
	Combined	**0.47**	**0.93**
Type IV	Self-Weight	-	-1.38
	PS + Self Weight	**-**	**2.62**
	Temperature	0.77	-0.86
	Temp. + Self Weight	0.77	-2.23
	Combined	**0.77**	**1.73**
Type V	Self-Weight	-	-2.17
	PS + Self Weight	**-**	**3.1**
	Temperature	1.47	-0.62
	Temp. + Self Weight	1.47	-2.79
	Combined	**1.47**	**2.5**

The AASHTO design gradient and the Lee's 2010 model were also applied to prestressed concrete beams in SAP2000. The maximum stresses from these gradients are displayed in Table 4.8 and the maximum deflections in Table 4.9.

While thermal gradient loading from the measured temperatures decreased the camber of the prestressed beams, both AASHTO and Lee (2010) increase this upward deflection. The beams experienced higher tensile stresses under the measured temperature gradient in all three

cases. The mid-span stress contours for the Type II, Type IV, and Type V under all three gradients are displayed in Figures 4.29, 4.30, and 4.31.

Table 4.8 – Maximum mid-span stress from AASHTO, Lee (2010), and measured thermal gradients

		Top Stress	Bottom Stress	Max Comp.	Location	Max Tension	Location
		[ksi]	[ksi]	[ksi]	-	[ksi]	-
Type II	AASHTO	0.53 (C)	3.9 (C)	3.9	Bottom Fiber	0.16	Top Flange
	Lee (2010)	0.09 (T)	3.8 (C)	4.3	Bottom Edge	0.09	Top Fiber
	Measured	0.67 (T)	3.8 (C)	2.39	Bottom Fiber	0.67	Top Fiber
Type IV	AASHTO	1.28 (C)	3.8 (C)	3.8	Bottom Fiber	-	-
	Lee (2010)	1.1 (C)	3.77 (C)	4.11	Bottom Edge	-	-
	Measured	0.06 (T)	3.9 (C)	3.9	Bottom Fiber	0.06	Top Edge
Type V	AASHTO	1.53 (C)	3.71 (C)	3.71	Bottom Fiber	-	-
	Lee (2010)	0.74 (C)	3.63 (C)	4.19	Bottom Edge	-	-
	Measured	1.91 (C)	3.93 (C)	3.93	Bottom Fiber	0.82	Top of Web

Table 4.9 – Maximum mid-span deflections from AASHTO, Lee (2010), and measured thermal gradients

		Max Lateral Displacement	Max Vertical Displacement
		[in]	[in]
Type II	AASHTO	-	1.83
	Lee (2010)	0.96	1.93
	Measured	0.47	0.93
Type IV	AASHTO	-	2.99
	Lee (2010)	1.4	3.39
	Measured	0.77	1.73
Type V	AASHTO	-	3.74
	Lee (2010)	1.49	4.2
	Measured	1.47	2.5

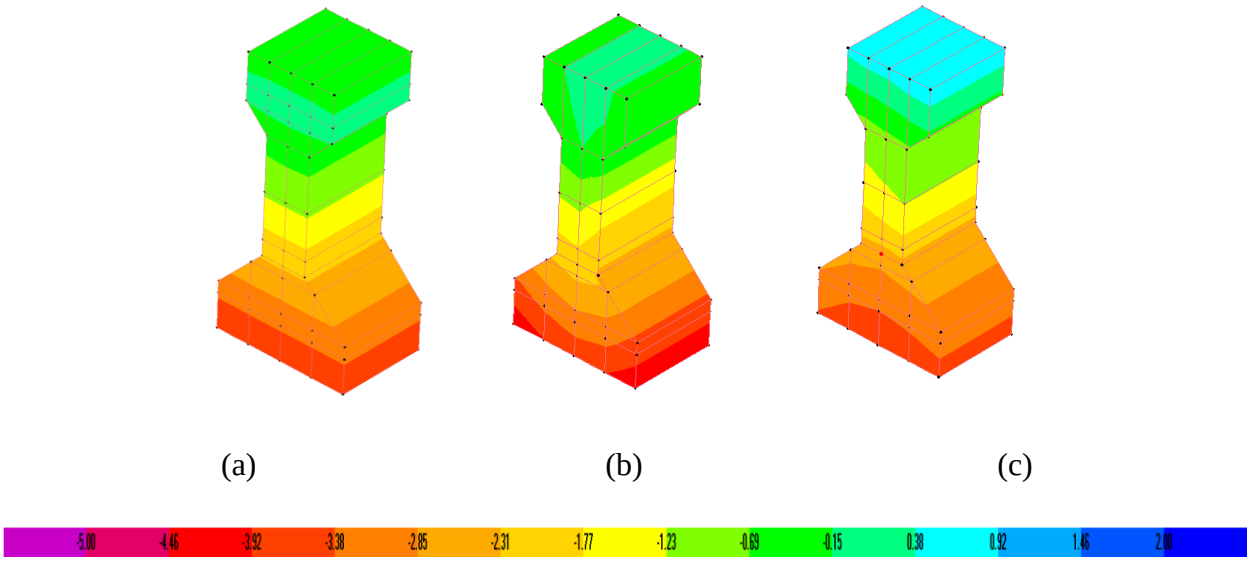

(a) (b) (c)

Figure 4.29 - Type II mid-span stress contours from (a) AASHTO, (b) Lee (2010), and (c) measured combined vertical and transverse temperature gradients

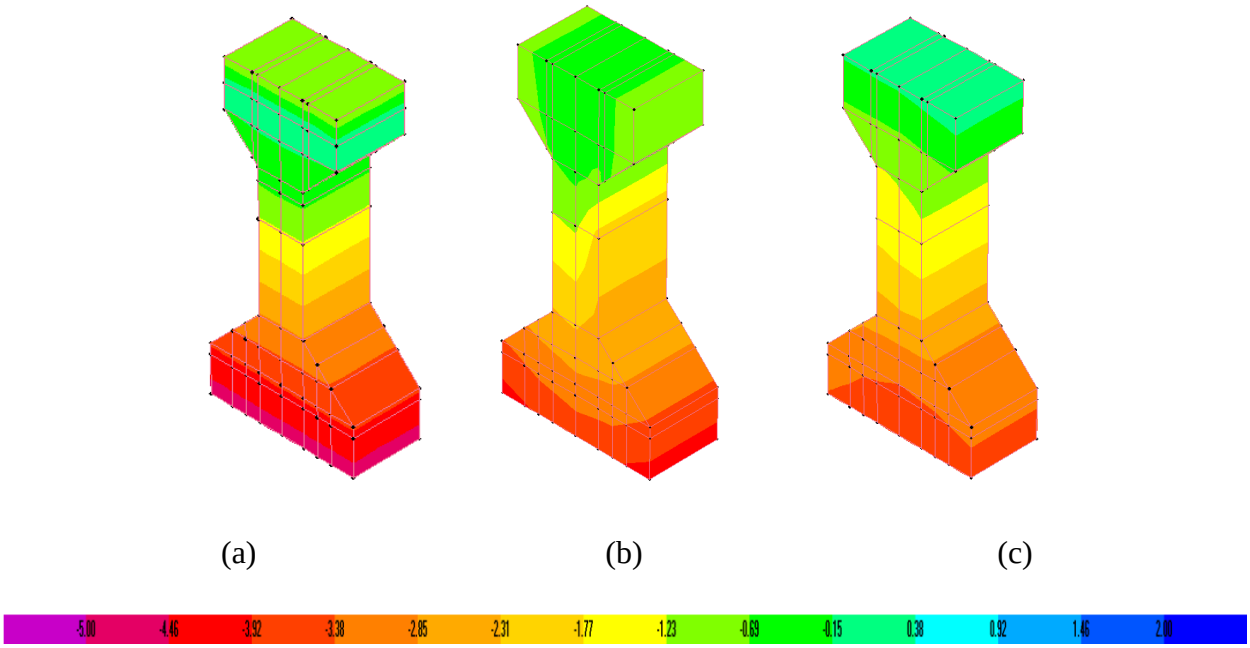

(a) (b) (c)

Figure 4.30 - Type II mid-span stress contours from (a) AASHTO, (b) Lee (2010), and (c) measured combined vertical and transverse temperature gradients

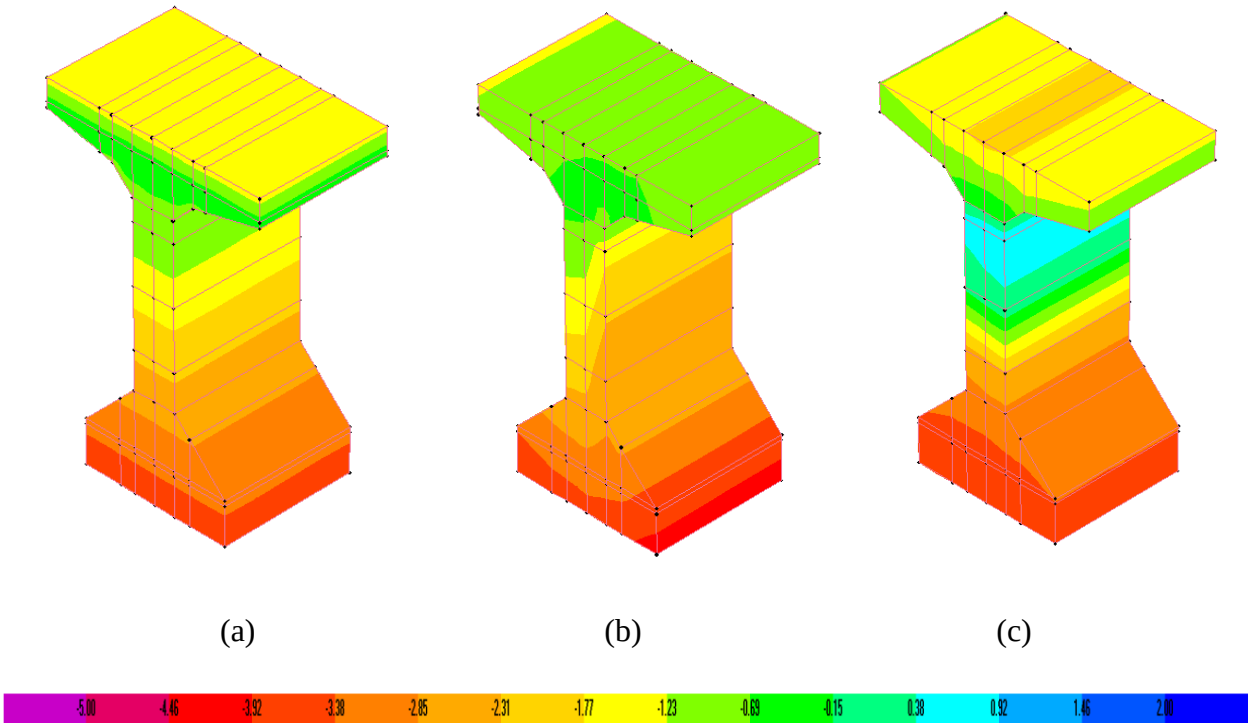

Figure 4.31 - Type V mid-span stress contours from (a) AASHTO, (b) Lee (2010), and (c) measured combined vertical and transverse temperature gradients

These figures better display how, when bridge girders experience non-linear temperature gradients, the resultant stresses can be somewhat unexpected. For example, the AASHTO design gradient increases the upward camber, yet instead of experiencing higher tensile stresses in the top fiber, the beams are actually in compression at the top fiber. Similarly, these gradients may cause an area of tension near the top of the web that is surrounded by compression zones in the top and bottom flanges. Even though the stress profile from the measured vertical gradient does not appear as extreme as the previous design gradients, the measured gradient is the only one that produced a tensile stress above the theoretical cracking stress of concrete ($7.5 \times f'_c{}^{0.5} = 671$ psi for 8 ksi concrete).

5. Conclusions and Recommendations

This research study investigated temperature gradients in AASHTO I-girders without wide top flanges and determined the environmental conditions that produce these gradients. Additionally, this research sought to understand the global response of concrete bridge girders to thermal gradients through three-dimensional finite element modeling. The results of this study indicate:

- Extreme heat is not necessarily the critical design condition when considering thermal gradients. A large daily temperature variation is the most important contributing factor. Low wind speeds and no precipitation also contribute.
- The current design standards do not accurately predict measured thermal gradients in the concrete I-shaped girders investigated in this study. When considering girders that have wider bottom flanges than top flanges, design vertical gradients are not representative of measurements in magnitude or shape.
- Based on three-dimensional modeling, the measured temperature gradients in this study increased tensile stresses in all three girders. In some cases, the tensile stresses in the concrete approached the cracking stress; however, these values do not warrant additional reinforcing steel or design procedures. Proper lateral bracing at all stages of construction should negate the effects of transverse thermal gradients enough to keep tensile stresses below the cracking limit.
- In the models, applied temperature gradients representative of those measured, decreased camber while the design gradients increased camber. Design engineers must be aware that camber may be less than the theoretical value if measured at mid-day before deck placement.

- The surface temperatures collected in this research were not reasonable measurements. Devices designed to collect surface temperatures while minimizing the effects of sunlight and ambient air temperature should be used for future research.
- Based on the results of this research, the vertical thermal gradient displayed in Figure 5.1 is recommended for AASHTO Type I, Type II, Type III, and Type IV girders in the pre-deck placement condition. The transverse thermal gradients for the pre-deck placement condition based on the data collected in this study for AASHTO Type I, Type II, Type III, and Type IV are displayed in Figure 5.2.

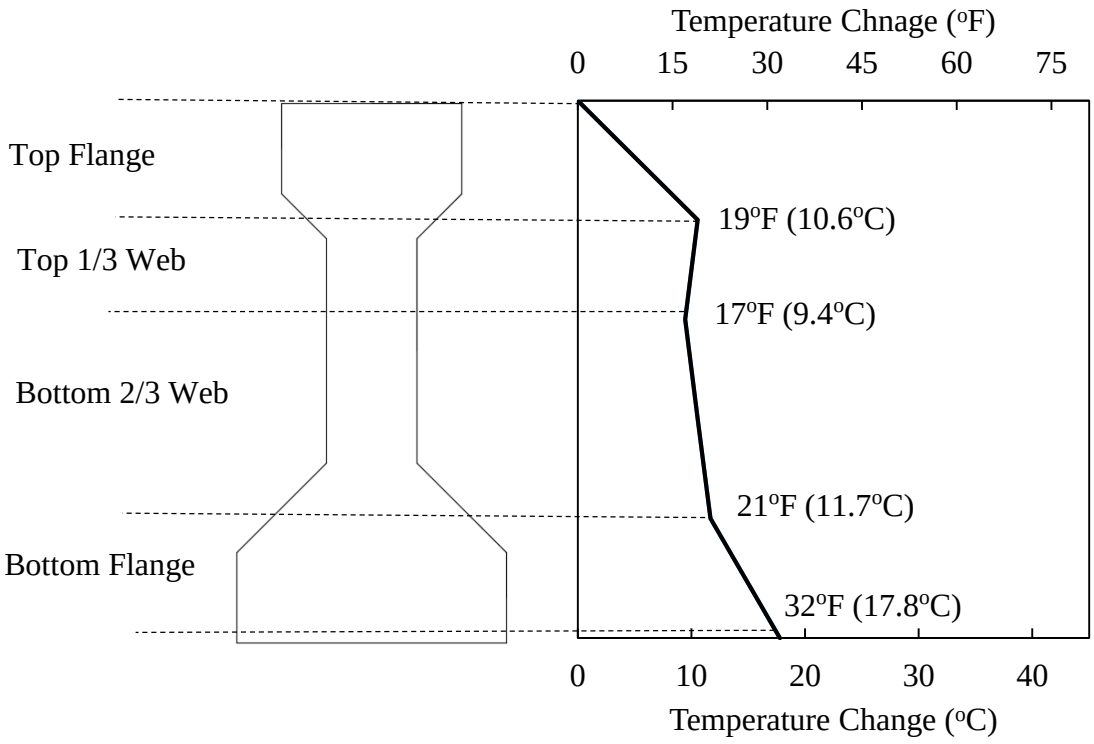

Figure 5.1 – Recommended vertical thermal gradient for AASHTO Type I – Type IV

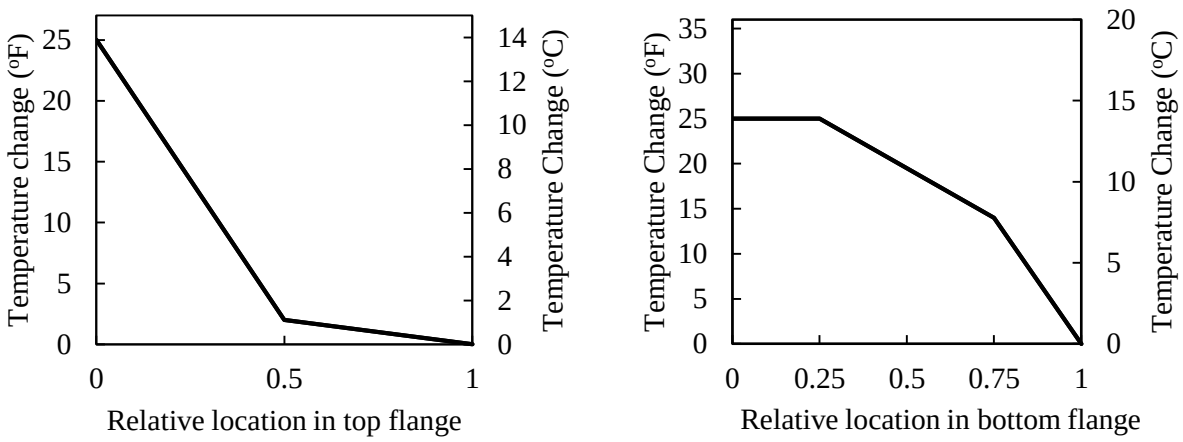

(a) (b)

Figure 5.2 – Recommended transverse thermal gradient for AASHTO Type I – Type IV for (a) top flanges and (b) bottom flanges

- The recommendations made by Lee (2010) for modifications to the vertical thermal gradient and addition of a transverse thermal gradient are reasonable for the design of AASHTO Type V girders and larger.
- An initial assumption of this research was that the most extreme vertical and transverse gradients would occur in concrete bridge girders before deck placement. This assumption should be researched further. It may be the case that both transverse and vertical gradients are worse during the service life of a bridge. The large surface area of bridge deck absorbs solar radiation and could cause large vertical gradients. Past research investigated the effects of bridge decks on the thermal gradients in other sections but this has not been done for I-girders. Even so, the added stability of a bridge deck may mean that the effects of thermal gradients are maximized during the construction phase even if the gradients themselves are not.

6. Works Cited

AASHTO. (2014). *AASHTO LRFD Bridge Design Specifications, U.S. Customary Units with 2015 interim revisions (7th edition)* American Association of State Highway and Transportation Officials (AASHTO).

AASHTO. (2012). *AASHTO LRFD Bridge Design Specifications, Customary U.S. Units (6th edition) with 2012 and 2013 interim revisions; and 2012 errata* American Association of State Highway and Transportation Officials (AASHTO).

AASHTO. (2007). *AASHTO LRFD Bridge Design Specifications, U.S. Customary Units.* American Association of State Highway and Transportation Officials (AASHTO).

AASHTO. (1989). *AASHTO LRFD Bridge Design Specifications, U.S. Customary Units.* American Association of State Highway and Transportation Officials (AASHTO).

ACI Committee 122. (2014). *122R-14 guide to thermal properties of concrete and masonry systems* American Concrete Institute.

ASHRAE. (2009). *2009 ASHRAE handbook - fundamentals (I-P edition)* American Society of Heating, Refrigerating and Air-Conditioning Engineers, Inc.

Barr, P., Stanton, J., & Eberhard, M. (2005). Effects of temperature variations on precast, prestressed concrete bridge girders. *Journal of Bridge Engineering, 10*(2), 186-194.

Cooper, P.I. (1969) The Absorption of Solar Radiation in Solar Stills. *Solar Energy*, 12 (3), 333-346.

Debbarma, S., & Saha, S. (2011). Behavior of pre-stressed concrete bridge girders due to time dependent and temperature effects. *First Middle East Conference on Smart Monitoring, Assessment and Rehabilitation of Civil Strucutres,*

Ghali, A., Favre, R., & Elbadry, M. (2006). *Concrete structures: Stresses and deformations: Analysis and design for serviceability*. CRC Press.

Gilliland, J. A., & Dilger, W. (1997). Monitoring concrete temperature during construction of the confederation bridge. *Canadian Journal of Civil Engineering, 24*(6), 941-950.

Hoffman, P., McClure, R., & West, H. (1980). *Temperature Studies for an Experimental Segmental Bridge* (No. FHWA/PA-82-002 Intrm Rpt.).

Hurff, J. B. (2010). Stability of precast prestressed concrete bridge girders considering imperfections and thermal effects. Ph.D. Georgia Institute of Technology, United States

Imbsen, R. A., & Vandershaf, D. E. (1984). Thermal effects in concrete bridge superstructures. *Transportation Research Record,* (950)

Kennedy, J. B., & Soliman, M. H. (1987). Temperature distribution in composite bridges. *Journal of Structural Engineering,* 113(3), 475-482.

Kim, K., Jeon, S., Kim, J., & Yang, S. (2003). An experimental study on thermal conductivity of concrete. *Cement and Concrete Research, 33*(3), 363-371.

Lee, J. (2011). Investigation of extreme environmental conditions and design thermal gradients during construction for prestressed concrete bridge girders. *Journal of Bridge Engineering,* 17.3(2011), 547-556.

Lee, J. (2010). Experimental and analytical investigations of the thermal behavior of prestressed concrete bridge girders including imperfections. Ph.D. Georgia Institute of Technology, United States

Li, D., Maes, M. A., & Dilger, W. H. (2004). Thermal design criteria for deep prestressed concrete girders based on data from confederation bridge. *Canadian Journal of Civil Engineering, 31*(5), 813-825.

Marion, W., & Wilcox, S. (1995). Solar Radiation Data Manual for Buildings, *NREL*

Meehl, G.A., & Tebaldi, C. (2004). More intense, more frequent, and longer lasting heat wave in the 21st century. *Science*, 305(5686), 994-997

Mehta, P. K., & Monteiro, P. J. M. (2006). *Concrete: Microstructure, properties, and materials* (3rd ed.) McGraw Hill.

Mirambell, E., & Aguado, A. (1990). Temperature and stress distributions in concrete box girder bridges. *Journal of Structural Engineering, 116*(9), 2388-2409.

Morabito, P. (1989). Measurement of the thermal properties of different concretes. *High Temperatures.High Pressures, 21*(1), 51-59.

Myers, J. J., Gopalaratnam, V., Nanni, A., Stone, D., & Earney, T. (2001). Precast I-girder cracking: Causes and design details. *Center for Infrastructure Engineering Studies and Missouri Department of Transportation Research, Development, and Technology Report Number 00-06,*

Nguyen, H., Stanton, J., Eberhard, M., & Chapman, D. (2015). The effect of temperature variations on the camber of precast, prestressed concrete girders. *PCI Journal,* 10.2(2005), 186-194.

Nilson, A. H., Darwin, D., & Dolan, C. W. (2004). *Design of concrete structures* (14th ed.). New York, NY: McGraw Hill.

Oesterle, R., Sheehan, M., Lotfi, H., Corley, W., & Roller, J. (2007). Investigation of red mountain freeway bridge girder collapse.

Potgieter, I. C., & Gamble, W. L. (1983). *Response of Highway Bridges to Nonlinear Temperature Distributions,* University of Illinois Engineering Experiment Station. College of Engineering. University of Illinois at Urbana-Champaign.

Priestley, M. (1976). Design thermal gradients for concrete bridges. *New Zealand Engineering, 31*(9), 213.

Roberts-Wollman, C. L., Breen, J. E., & Cawrse, J. (2002). Measurements of thermal gradients and their effects on segmental concrete bridge. *Journal of Bridge Engineering, 7*(3), 166-174.

Saetta, A., Scotta, R., & Vitaliani, R. (1995). Stress analysis of concrete structures subjected to variable thermal loads. *Journal of Structural Engineering, 121*(3), 446-457.

Schwartz Jr, H. G. (2010). Adaptation to the impacts of climate change on transportation. *Bridge, 40*(3), 5-13.

Thepchatri, T., Johnson, C. P., & Matlock, H. (1977). *Prediction of Temperature and Stresses in Highway Bridges by a Numerical Procedure using Daily Weather Reports,* (No. FHWATX-77-23-1 Intrm Rpt.). The Center.

Valore Jr, R. C. (1980). Calculation of U-values of hollow concrete. *Concrete International,*

Yargicoglu, A., & Johnson, C. P. (1978). Temperature induced stresses in highway bridges by finite element analysis and field tests.